Contrib Mineral Petrol (2010) 160:511–531
DOI 10.1007/s00410-010-0491-5

ORIGINAL PAPER

Trace element composition of igneous zircon: a thermal and compositional record of the accumulation and evolution of a large silicic batholith, Spirit Mountain, Nevada

Lily L. Claiborne · Calvin F. Miller · Joseph L. Wooden

Received: 2 January 2009 / Accepted: 15 January 2010 / Published online: 10 February 2010
© Springer-Verlag 2010

Abstract Hafnium, U, Th, and REE content of zircons from the Spirit Mountain batholith in southern Nevada correlate with calculated temperatures from the Ti-in-zircon thermometer to support field and petrologic evidence of rejuvenation of crystal mush and melt extraction events during the 2-million year accumulation of the granitoid batholith. Marked variation in zircon composition from sample to sample, from grain to grain within individual samples, and from zone to zone within individual grains documents in detail a history of fluctuating conditions with repeated episodes of replenishment, reheating, crystal mush rejuvenation, fractional crystallization, and melt segregation. The zircons exhibit compositional and thermal variability indicative of variations in host melt composition due to (1) melt rejuvenation, mixing, and fractionation (2) coeval growth of other REE-rich accessory minerals, and possibly (3) fluctuation in fO_2.

Keywords Zircon · Trace elements · Granite · Crystal mush · Fractionation · Rejuvenation · Ti-in-zircon thermometer

Communicated by T. L. Grove.

Electronic supplementary material The online version of this article (doi:10.1007/s00410-010-0491-5) contains supplementary material, which is available to authorized users.

L. L. Claiborne (✉) · C. F. Miller
Department of Earth and Environmental Sciences, Vanderbilt University, Nashville, TN 37235, USA
e-mail: lilyclaiborne@gmail.com

J. L. Wooden
Department of Geological and Environmental Sciences, Stanford University, Stanford, CA 94305, USA

Introduction

It has become evident that many plutonic and volcanic systems accumulate and evolve over protracted periods of time, with complex histories that require frequent replenishment in order to attain the extended histories recorded in crystal populations (Wiebe and Hawkins 2004; Davies et al. 1994; Reid et al. 1997; Brown and Fletcher 1999; Schmitt et al. 2003; Vazquez and Reid 2002; Charlier et al. 2005; Miller and Wooden 2004; Glazner et al. 2004; Coleman et al. 2004; Walker et al. 2007). In these repeatedly replenished systems, temperature, quantity, composition and location of melt must fluctuate through time as zones of crystal mush and rigid sponge (Hildreth 2004) are reheated and potentially rejuvenated by introduction of new melt, mix with other magmas, crystallize and fractionate. Crystals within these systems are often recycled by entrainment in new magma (Miller and Wooden 2004; Bacon and Lowenstern 2005; Walker et al. 2007) potentially causing dissolution followed by crystallization, and recording these fluctuating conditions throughout the growth history of the crystal (e.g., Davidson et al. 2007; Vazquez and Reid 2002; Harper et al. 2004; Claiborne et al. 2006a, b; Hanchar and Miller 1993). Zoned crystals, then, document the sequence and timing of changing environments within the magmatic system and can provide clues to the magmatic processes involved in accumulation and evolution of magmatic systems with protracted histories.

Due to its refractory nature and low elemental diffusivities (e.g., Cherniak et al. 1997a; Cherniak et al. 1997b; Cherniak and Watson 2003) and resulting ability to retain its compositional zoning through time and varying conditions, zircon is particularly invaluable for investigating the evolution of long-lived and complex magmatic silicic systems. Growth and dissolution of accessory phases,

including zircon, act as a primary control over the trace element budget of the magmas (e.g., Wark and Miller 1993; Hoskin and Schaltegger 2003; Claiborne et al. 2006a). The trace element composition of these minerals, then, can reflect the trace element budget in the melt at the time of crystallization. The recent development of methods for the Sensitive High Resolution Ion Microprobe-Reverse Geometry (SHRIMP-RG) that enable high-precision in situ analysis of trace element composition of zones within zircons, including Ti, Hf, and rare earth elements (REE) (Mazdab and Wooden 2006), combined with SHRIMP-RG in situ U–Pb dating and careful application of the Ti-in-zircon thermometer (Watson et al. 2006; Ferry and Watson 2007), allows unprecedented insight into both the utility of the temporal–thermal–compositional record retained in igneous zircon and the long-term evolution of silicic crustal systems (Claiborne et al. 2006a; Bolhar et al. 2008; Marks et al. 2008; Bindeman et al. 2006; Vazquez et al. 2008). In this study, we seek to evaluate the integrity of zircon elemental compositions as tracers of magmatic processes by integrating the zircon record with existing information for a well-characterized plutonic system, and then apply that record to refine our understanding of the accumulation and evolution of large silicic systems.

The Spirit Mountain batholith (SMB) in southern Nevada provides an ideal example of one of these long-lived silicic systems, with zircons (U–Pb SHRIMP studies) documenting nearly 2 million years of magma accumulation and evolution (Walker et al. 2007). Field evidence as well as zircon geochronology suggests repeated episodes of recharge, fractionation, and some magma mixing (Walker et al. 2007). A relatively large, high-silica leucogranite cap overlies a large volume of cumulate granite, both of which apparently accumulated over the lifetime of the magmatic system, as injections of new magma rejuvenated crystal mushes and as fractionated melt segregated from the continuously accumulating pockets of crystal mush and amassed in the roof zone (Walker et al. 2007; Claiborne et al. 2006a; i.e., Bachmann and Bergantz 2004). In this context, the term "cumulate" is used to indicate a magma or resultant rock from which some portion of the interstitial melt has been extracted, leaving a crystal-rich residue or cumulate. Zircons selected from samples of both the fractionated leucogranites and the cumulate granites to quartz monzonites were analyzed by SHRIMP-RG, and provide detailed information revealing the thermal–compositional history of the magmatic processes involved in the construction of the patchwork batholith.

Zircon growth and trace element composition

Zircon growth in a magma requires sufficiently low temperatures and sufficiently high Zr content for saturation, and relatively low rates of diffusion in the melt require that these conditions be maintained for some extended period of time (Watson 1996). Large uniform zones in zircons represent episodes of growth in a saturated environment and reflect magmatic conditions and composition (Hoskin 2000; Fowler et al. 2002). Due to relatively slow growth rates (Watson 1996), zircon crystals likely behave as essentially inert when they encounter rapid (moment to thousands of year) changes in melt conditions, failing to record either rapid fluctuations or events such as those thought to trigger volcanic eruptions (Sparks et al. 1977; Pallister et al. 1992; Eichelberger and Izbekov 2000; Wark et al. 2007). Oscillatory zoning represents kinetic effects at the crystal-melt interface, dependent on ordering in the melt by polymerization and often promoting local supersaturation and disequilibrium, rather than rapid changes in the composition or conditions in the bulk melt (Hoskin 2000; Hoskin and Schaltegger 2003; Fowler et al. 2002; Shore and Fowler 1996; Putnis et al. 1992). Current limitations on analysis introduced by the spot size of in situ analytical instruments make it difficult to delineate trace element compositions of individual oscillatory zones, particularly those less than a few microns thick. However, analyses of entire bands of oscillatory zoning are likely representative of the average composition and conditions of the magma at the time of crystal growth.

Because hafnium is nearly identical in size and charge to zirconium, the two behave nearly identically. Zircon, therefore, is essentially a zircon-hafnon solid solution, with most natural zircons containing between 1 and 2 wt% HfO_2 (Ahrens and Erlank 1969; Heaman et al. 1990; Bea et al. 2006; Belousova et al. 2002; Hoskin and Schaltegger 2003; Claiborne et al. 2006a). As zircon is the primary reservoir for the crust's Hf, growth of zircon controls the Hf composition of any melt. As zircon grows, both the Zr and Hf concentrations in the magma will decrease. However, this growth preferentially incorporates Zr over Hf and therefore leads to a decrease in the Zr/Hf of the remaining melt. This process leads to increasing Hf concentration in growing zircon crystals that corresponds to increasing fractionation of the magma (Claiborne et al. 2006a). Trace elements found in reasonably measureable quantities in natural zircon include U, Th, Ti, REE, Sc, Y and P. Zircons are generally heavy rare earth enriched and light rare earth-depleted with negative Eu anomalies and strong positive Ce anomalies (Hoskin and Schaltegger 2003; Claiborne et al. 2006a).

Recent work by Watson and Harrison (2005), Watson et al. (2006) and Ferry and Watson (2007) has demonstrated that incorporation of Ti into zircon depends primarily on temperature, and that Ti concentration of zircon can therefore be used to estimate the magma temperature at the time of crystallization. Accurate calculation of

temperature requires knowledge of the activity of TiO_2 (a_{TiO_2}) and SiO_2 (a_{SiO_2}) in the melt at the time of crystallization. This can prove an impediment to use of the thermometer, as zircon studies have shown that individual grains often exhibit complex histories with growth from different melts at different times; in general, zircons often were not in equilibrium with the melt or glass that was their final host (Miller and Wooden 2004; Bacon and Lowenstern 2005; Walker et al. 2007). Evolution of the melt during crystallization of a magma or events such as rejuvenation and magma mixing will likely result in changes in a_{TiO_2} and a_{SiO_2}. However, expected simultaneous changes in a_{TiO_2} and a_{SiO_2} have counter-effects on the thermometer, with one balancing the effect of the other, and growth of Ti-bearing minerals may roughly buffer a_{TiO_2} during melt evolution (Watson et al. 2006; Ferry and Watson 2007). Therefore, careful consideration of the history of the magma and the system in question can allow application of the thermometer with reasonable confidence (see "Methods" for further discussion).

Geologic background

The Spirit Mountain batholith

The Spirit Mountain batholith formed during the Miocene as part of an extensive episode of magmatism prior to and during crustal extension in the northern Colorado River Extensional Corridor of southernmost Nevada (Fig. 1) (Walker et al. 2007; Faulds et al. 1995; Gans and Bohrson 1998; Howard et al. 1996). Uplift and 40° to 50° westward tilting (Faulds et al. 1992) exposed a cross-section of the batholith from the roof to deep levels, providing a 250 km^2 record of the construction of a composite silicic intrusive system (Fig. 2; Walker et al. 2007). Field relations suggest that the batholith accumulated by repeated injection of subhorizontal sheets from which crystal poor, fractionated melt commonly was extracted and ascended toward the roof zone, leaving a crystal rich cumulate behind to amalgamate with existing crystal mush. In situ U–Pb dating of zircons by SHRIMP-RG indicates a nearly 2-million year history for this accumulation process (~17.5–15.3 Ma). Zircons from single samples commonly exhibit much of the total age range, suggesting that new pulses of magma recycled existing zircons by incorporating less solidified portions of the existing intrusion (Walker et al. 2007).

Walker et al. (2007) subdivide the Spirit Mountain batholith into the *Spirit Mountain granite* (~16–17 Ma, described below), which is volumetrically dominant and the subject of this study, and several other smaller units that range from slightly older to slightly younger. Here, we briefly describe these other units. Based upon field relations, a felsic granite *roof unit* (~17.4 Ma) exposed along one portion of the roof appears to be the oldest unit. It is intruded by even more felsic leucogranites of the Spirit Mountain granite. The north-striking, E-dipping *Newberry Mountains dike swarm* marks the final stage of Spirit Mountain magma emplacement at ~15.3 Ma. It includes abundant rhyolite porphyries and subordinate intermediate to felsic dikes that brittlely cut all the other units. The other units all intrude deeper parts of the Spirit Mountain granite and are 16.0 Ma or slightly younger in age. The *Mirage granite* is relatively fine grained and comprises a discrete pluton. *Dioritic sheets*, which constitute a very small fraction of the total batholith, are the only direct manifestation of mafic input, although small mafic enclaves are common throughout the older, coarse cumulate granites and quartz monzonites of the Spirit Mountain granite. Sheets of *fine-grained granite* have compositions and textures consistent with granitic replenishments, essentially quenched in situ without fractionation. Full descriptions of the various rock units, field relationships, and zircon geochronology can be found in Walker et al. (2007).

The cross-sectional view of the Spirit Mountain granite afforded by tilting reveals a fairly consistent textural and compositional sequence from west to east (top to bottom) that is broken up by younger intrusions that generally

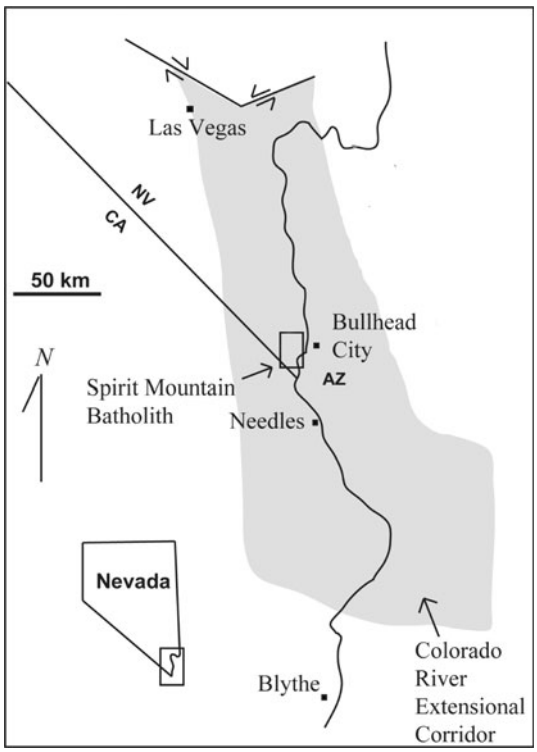

Fig. 1 Map showing the study location, the Spirit Mountain batholith in the Colorado River Extensional Corridor of southern Nevada and western Arizona

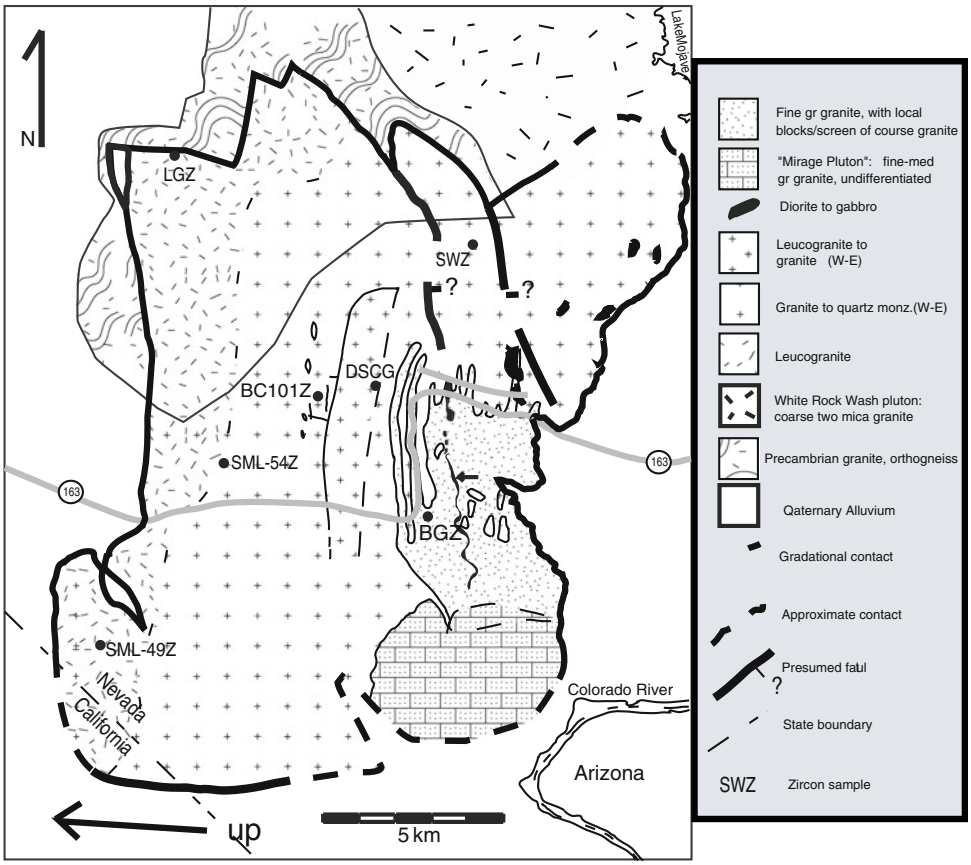

Fig. 2 Geologic map of the Spirit Mountain batholith showing locations of samples used in this study (modified from Walker et al. 2007)

repeat the stratigraphy of the larger body. This unit, which constitutes almost 90% of the batholith, grades from a high-silica leucogranite at the roof (up to 79 wt.% SiO_2) through granites into quartz monzonite at the lowest exposed levels (down to 61 wt.% SiO_2). These rocks contain a uniform mineral assemblage, with variable modal abundances, that includes alkali feldspar, plagioclase, quartz, biotite, sphene, zircon, apatite, oxides and allanite or chevkinite (fluorite is sparsely present in leucogranites). They exhibit increasingly prominent magmatic foliation with depth, manifested most strongly by alkali feldspars that define an initially sub-horizontal fabric. Individual intrusions within the Spirit Mountain granite, where identifiable, also appear to have been originally sub-horizontal, with vertical to sub-vertical dikes feeding the base of these sheets and transporting segregated melt upward from the top. Enclaves of fine-grained diorite are common in the lower half of the granite unit, and increase in both size and abundance with depth. Our studies (Walker et al. 2007; Claiborne et al. 2006a) support previous work (Hopson et al. 1994), suggesting that the extensive, foliated, coarser-grained granite represents residual cumulate and the high-silica leucogranite adjacent to the roof represents complementary fractionated melt. However, complex age and field relations suggest that the batholith formed by repeated episodes of intrusion, fractionation accompanying crystal growth, and segregation of interstitial melt (Walker et al. 2007; Claiborne et al. 2006a). These segregated melts were repeatedly injected into the roof zone as dike-fed sheets, eventually accumulating the >55 km^2 leucogranite cap, leaving melt-poor cumulate residues in the lower portions of the body (Walker et al. 2007; Claiborne et al. 2006a).

Petrology, geochemistry and zircon saturation temperatures

The leucogranites are composed of ~40–50% white alkali feldspar, 30–40% quartz, 10–30% sodic plagioclase, ~1% biotite, and accessory apatite, allanite, sphene, zircon, fluorite and opaque oxides. They range in SiO_2 from 76 to 79 wt%, with very low Sr and Ba concentrations (mostly 5–50 and 20–100 ppm, respectively), strong light to middle REE depletions (up to a factor of 10) compared to other granitoids in the batholith, large negative Eu anomalies (Walker et al. 2007), and low Zr/Hf (Claiborne et al. 2006a), all of which suggest that these high-silica leucogranites are the product of fractional crystallization (Table 1). The leucogranite grades with depth into a coarser, less felsic granite with pink alkali feldspars, increasing biotite abundance and decreasing abundance of quartz. This coarse granite, which extends downward for ~3 km, averages

~20–35% plagioclase, 30–40% alkali feldspar, 15–30% quartz, 5–8% biotite, up to 1% sphene and accessory apatite, allanite, zircon and opaque oxides. The coarse grained granite grades downward into magmatically foliated quartz monzonite that is poorer in quartz and richer in biotite. The quartz monzonite is coarse-grained, with 40–50% alkali feldspar, 30–35% plagioclase, 10–15% biotite, 5–15% quartz, up to ~1% sphene and accessory apatite, allanite, zircon and opaque oxides. These less felsic granites are enriched in light REE (up to 600 times chondrite) and exhibit small Eu anomalies relative to the leucogranites and flat middle to heavy REE/chondrite patterns (Table 1), suggesting that they represent the cumulate residues of fractional crystallization (Walker et al. 2007).

Textures, field relations and petrography suggest that the fine-grained granite unit (represented by sample BGZ) may represent something like the primary input liquid into the batholith, and that the leucogranites [represented by samples LGZ and others (Walker et al. 2007)] likely represent interstitial liquid segregated from cumulate mush. The zircon saturation temperatures calculated using Harrison and Watson (1983) for these two units, 785 and 734°C, respectively (Table 2), may represent reasonable constraints on zircon growth in these two types of melts essential to the assembly of the Spirit Mountain batholith. However, depending on the amount of crystal-melt fractionation that occurred in these prior to zircon growth, the temperatures may be underestimates. Because the cumulate granite compositions do not closely resemble melt compositions, calculated zircon saturation temperatures are not meaningful for these rocks.

Methods

Sample preparation and analytical methods

Six samples from the Spirit Mountain granite unit were selected for detailed zircon trace element analysis (see Fig. 2 for sample locations). Samples SWZ, DSCG, and BC101Z were selected as representative cumulates based on texture, chemical composition, mineralogy, and field relations. DSCG was collected from a relatively young portion of the unit (see Fig. 2). Samples LGZ and SML49Z were selected as representative leucogranites using the same criteria. Sample SML54Z represents a transitional granite, intermediate in composition, texture, and location between cumulates and leucogranites (Fig. 2).

Each ~5 kg sample was crushed to pass through a 500 μm mesh. An initial density separation was performed using hydraulic separation, followed by density separation with heavy liquids of density 2.85, magnetic separation and hand picking of at least 100 zircon grains per sample from the least magnetic fraction. Thirty to fifty zircons from each sample were then mounted in epoxy and ground near the center of the grains and polished. Due to variable sizes of crystals on any given mount, uniform polishing reveals different depths in different sized grains. Imaged and analyzed "cores" or "centers" of grains, therefore, often represent the center of the cross-sectional surface that was revealed, not necessarily the very center of the grain. Grains were then imaged in reflected light on a petrographic microscope and by cathodoluminescence (CL) on the JEOL JSM 5600 scanning electron microscope at the USGS/Stanford Microanalytical Laboratory.

The zircons were analyzed using the USGS/Stanford Sensitive High Resolution Ion Microprobe, Reverse Geometry (SHRIMP-RG). Spots for trace element analyses were selected based on zoning visible in CL images and in an attempt to avoid inclusions visible in reflected light images, with preference for locations that had been previously analyzed for U–Pb ages. In these cases, mounts were repolished and coated following U–Pb analyses. Variations in technique between the first and second trace element analysis session were due to the evolving state of the methodologies (Mazdab and Wooden 2006). In the first of two sessions (samples LGZ and SWZ only, September 2005), the trace element routine included $^{31}P^+$, $^{40}Ca^+$, $^{48}Ti^+$, $^{49}Ti^+$, $^{56}Fe^+$, $^{89}Y^+$, $^{172}Yb^{16}O^+$, $^{180}Hf^{16}O^+$, $^{232}Th^{16}O^+$ and $^{238}U^{16}O^+$, in addition to $^{30}Si^+$, $^{96}Zr^+$ and $^{90}Zr_2^{16}O^+$ reference peaks. $^{49}Ti^+$ was selected over more abundant $^{48}Ti^+$ for calculation of concentrations to avoid interference from $^{96}Zr^+$. For the second session (all six samples, March 2006), $^{45}Sc^+$, $^{139}La^+$, $^{140}Ce^+$, $^{146}Nd^+$, $^{147}Sm^+$, $^{153}Eu^+$, $^{157}Gd^{16}O^+$, $^{159}Tb^{16}O^+$, $^{163}Dy^{16}O^+$, $^{165}Ho^+$, $^{167}Er^{16}O^+$, $^{169}Tm^{16}O^+$, and $^{175}Lu^{16}O^+$ were added to the analytical routine, thus completing the suite of REE. The analyses included Pr, but results were considered unreliable due to potential hydride interference from the $^{140}Ce^1H^+$ peak. For Yb, Gd, Tb, Dy, Er, Tm, Lu, Hf, Th and U, the oxide peaks rather than the element peaks were used due to their greater ion production during sputtering. In the first session, each measurement consisted of one block of three cycles. During the second session, we generally ran two cycles and in a few cases one. Each cycle represents a sequential stepping through the entire mass range from low to high mass. Data reduction involved averaging raw counts for all cycles and then normalizing to the average $^{30}Si^+$ count rate. This normalization minimizes variations caused both by drift in the primary current and by time-dependent ionization phenomena related to sputtering. Normalized count rates from the unknowns were compared to comparable measurements of standard zircon CZ3 which were calibrated against a set of synthetic REE and Ti-bearing zircons to determine absolute elemental concentrations. These synthetic zircons were grown using a

Table 1 Whole-rock geochemistry of samples from the Spirit Mountain batholith used in this study

Sample ID	SML49Z (leucogranite)	LGZ (leucogranite)	SML54Z (transitional/ leucogranite)	BC101Z (cumulate)	DSCG (cumulate)	SWZ (cumulate)	BGZ (fine-grained granite)
SiO_2	77.37	76.80	75.57	70.84	68.88	63.19	73.83
Al_2O_3	12.46	12.65	13.09	14.77	15.53	17.64	14.23
Fe_2O_3	0.68	0.92	1.19	2.37	2.94	4.10	1.56
MnO	0.05	0.05	0.05	0.06	0.06	0.09	0.04
MgO	0.09	0.10	0.28	0.69	0.85	1.35	0.34
CaO	0.43	0.67	0.78	1.71	2.18	2.73	1.48
Na_2O	4.08	3.92	3.67	4.06	4.00	4.70	3.63
K_2O	4.69	4.75	5.12	4.95	4.84	5.07	4.62
TiO_2	0.12	0.13	0.20	0.43	0.53	0.87	0.23
P_2O_5	0.04	0.02	0.05	0.13	0.18	0.27	0.05
Rb	204	236	157	131	98	83	169
Sr	17	27	89	272	356	551	243
Ba	37	92	326	886	1,323	1,850	1,009
Cs	0.7	0.7	0.8	1.0	0.7	0.3	0.8
Ta	3.2	3.33	1.5	1.74	1.73	1.11	0.84
Nb	43.8	38.3	23.4	24.3	22.0	19.2	15.3
Tl	0.88	0.86	0.82	0.82	0.51	0.38	0.63
Hf	4.2	4.1	4.2	5.8	7.7	12.3	4.4
Zr	99	83	127	229	312	557	150
Y	19	18	16	28	43	26	19
V	<5	5	11	29	37	57	15
Th	20.8	19.1	17.1	17.4	9.26	8.91	14.8
U	2.89	2.67	1.34	1.81	1.26	1.09	1.14
Ga	20	31	18	28	20	22	27
La	36	46.7	36.5	106	73.3	103	54.1
Ce	63	77.7	73.2	187	153	210	101
Pr	5.77	6.39	7.81	17.8	16.7	21.7	9.75
Nd	15.7	17.9	23.7	60.0	57.0	79.5	34.5
Sm	2.49	2.76	3.93	9.41	10.0	12.0	6.07
Eu	0.202	0.235	0.546	1.52	1.64	2.41	1.04
Gd	1.65	2.16	2.52	7.06	7.83	7.86	4.35
Tb	0.38	0.43	0.47	1.18	1.30	1.15	0.75
Dy	2.48	2.60	2.61	5.98	7.14	5.65	3.86
Ho	0.58	0.58	0.55	1.16	1.34	1.00	0.78
Er	2.15	2.18	1.81	3.64	4.15	3.06	2.46
Tm	0.387	0.400	0.298	0.534	0.636	0.442	0.372
Yb	2.62	2.67	1.89	3.06	3.80	2.92	2.29
Lu	0.395	0.404	0.272	0.393	0.460	0.414	0.337
Sn	1	1	1	2	2	1	<1
Be	3	6	2	3	2	2	2
Ge	1.7	2.3	1.4	1.1	1.2	1.0	1.4
Bi		0.8		0.8	1.5	0.2	0.2
Th/U	7.20	7.15	12.76	9.62	7.37	8.20	13.01
Zr/Hf	23.57	20.46	30.24	39.55	40.42	45.12	34.12

Oxides are reported in wt.% and elements are reported in ppm (from Walker et al. 2007)

Table 2 Zircon and rutile saturation temperatures and their factors for calculation for samples with assumed near-liquid compositions (equations from Watson and Harrison 1983 and Hayden and Watson 2007; whole-rock geochemical data from Walker et al. 2007)

Sample	Zr (ppm)	*M* factor	Zircon saturation *T* (°C)	Ti (ppm)	FM factor	Rutile saturation *T* (°C)
BGZ	*150*	*1.39*	*785*	*1,352*	*1.68*	*782*
LGZ	*83*	*1.41*	*734*	*753*	*1.57*	*734*
SML52	137	1.39	777	970	1.57	756
BW47	47	1.35	696	331	1.43	673
SML63C	186	1.36	806	1,249	1.61	777
SML47	83	1.39	736	847	1.54	745
SML49Z	*99*	*1.40*	*749*	*693*	*1.52*	*728*
SML76	123	1.41	767	428	1.53	690
SML132	93	1.41	744	428	1.53	690
SML74	111	1.39	759	706	1.52	730
SML130	92	1.39	744	706	1.52	730
BW24	152	1.32	792	965	1.48	757
SML129Z	116	1.38	764	739	1.51	734
SML73	128	1.38	772	739	1.51	734
SML69	68	1.39	721	513	1.49	705
SML71	131	1.39	773	773	1.53	737
SML120Z	202	1.39	811	773	1.53	737
SML67	114	1.32	766	607	1.43	720
SML78	96	1.35	750	501	1.45	704
SML133	165	1.35	796	501	1.45	704

Samples are listed in order of increasing silica content, and all samples are leucogranites, with >76 wt.% SiO_2, except BGZ, which is a fine-grained granite with 73.83 wt.% SiO_2 (Walker et al. 2007). M and FM are factors that account for zircon and rutile solubility dependence on melt composition (Watson and Harrison 1983; Miller et al. 2003; Hayden and Watson 2007). Italicized entries indicate samples with zircons included in this study

technique modified from Hanchar et al. (2001) and were independently analyzed by electron microprobe (Mazdab and Wooden 2006).

Application of the Ti-in-zircon thermometer

Watson et al. (2006) and Watson and Harrison (2005) described the dependence of Ti concentration in zircon on crystallization temperature, and defined a thermometer based on experimental results and well-characterized natural samples. This initial form of the thermometer assumed that the melt from which the zircon grows was saturated in quartz, but allowed for variability in a_{TiO_2}. Ferry and Watson (2007) revised the thermometer calculation to allow for undersaturation in both rutile and quartz by incorporating a_{TiO_2} and a_{SiO_2}, following the equation:

$$T(\mathrm{K}) = \frac{-4{,}800 \pm 86}{\log \mathrm{Ti(ppm)} + \log a_{SiO_2} - \log a_{TiO_2} - (5.711 \pm 0.072)}.$$

Accurate application of this thermometer requires knowledge of a_{TiO_2} and a_{SiO_2} at the time of zircon crystallization. This can be an impediment to use of this tool, as it can be difficult to constrain activities at the time of zircon growth. Zircons often were not in equilibrium with their final host magma, and crystallization will likely cause a_{TiO_2} and a_{SiO_2} to change during the evolution of a magma. Careful consideration of the system specific melt compositions and mineral assemblages, effects of melt evolution during crystallization or mixing on these activities and the effect of changes in activity with time on the thermometer can allow useful application of the Ti-in-zircon thermometer, even when activities cannot be definitively identified from the rocks themselves. In these cases of undersaturation in either quartz or rutile, unless it can be determined that a volcanic zircon is cognate to a glass with which it is in contact and for which a_{TiO_2} and/or a_{SiO_2} are known, calculated temperatures must be considered estimates.

The configuration of the temperature equation is such that a similar magnitude overestimate or underestimate of both activities will tend to offset resulting errors in estimated *T* (Ferry and Watson 2007). Overestimating the a_{SiO_2} will result in an overestimate of temperature, while overestimating the a_{TiO_2} will result in an underestimate of temperature. In natural compositions, it is likely that both would increase with fractionation until reaching saturation.

Textures of the cumulates suggest that significant amounts of crystallization occurred before the magmas saturated in quartz, although considering zircon saturation temperatures it may be that much of the zircon grew coeval with quartz. The evolved nature of even the putative primary magmas (BGZ) necessitates a relatively high a_{SiO_2}. As we cannot be certain how these compositions varied and considering the ubiquity of quartz in these samples, we have held a_{SiO_2} constant at 1, thus maximizing temperature estimate. Coexisting Ti-bearing phases (sphene and potentially ilmenite) indicate a_{TiO_2} was not low (Hayden and Watson 2007; table 4), although few natural magmas are rutile saturated. Rutile saturation temperature was calculated using the equation of Hayden and Watson (2007) and compared with zircon saturation temperatures (Harrison and Watson 1983; Miller et al. 2003; Hanchar and Watson 2003) for samples with assumed near-liquid compositions, such as the leucogranites and putative primary input melt BGZ (Table 2). This comparison suggests that these magmas were near rutile saturation at reasonable temperatures for zircon growth, supporting our assumption of a relatively high a_{TiO_2}, which we held constant at 0.7. Calculated T_{TiZ} for samples LGZ and SWZ have been amended from those previously reported in Claiborne et al. (2006a), reflecting recalibration of the Watson et al. (2006) thermometer by Ferry and Watson (2007). The new, revised temperatures are slightly higher, by approximately 5–15°C and are considered in the data interpretations but are not re-reported herein.

A moderate pressure dependence of the Ti-in-zircon thermometer has been suggested by Ferry and Watson (2007) and Ferriss et al. (2008) (~5–10°C/kb). This implies that calculated temperatures from the Ferry and Watson formulation (calibrated at 10 kb) could be tens of degrees too high for the shallow crust and tens of degrees too low at very deep crust or upper mantle pressures. Because the Spirit Mountain batholith was emplaced in the upper crust, this suggests that our calculated temperatures may be systematically too high. However, it is very unlikely that the large *relative* differences in temperature that we estimate are not real, and the generally reasonable magmatic temperature range would still apply even with a downward correction.

Results

Zircon zoning in CL images

Zircons are abundant in both leucogranite and cumulate samples, and identified grains range in size up to our maximum retrievable size, 500 μm in length. Grains are generally euhedral, prismatic, and often contain mineral and/or melt inclusions. CL imaging of the zircons reveals distinct euhedral zoning, visible as discrete zones and as bands of oscillatory zoning. Different samples have populations with distinctly similar zoning patterns, although it was not possible to definitively match zoning stratigraphy or characteristics among grains from the same samples or among grains of the same age. Although we do not ultimately base our interpretations on the appearance of the zoning or take zoning as a proxy for composition, relative brightness of zones does appear to correlate with Ti, Hf, U, Th and REE concentrations, with dark zones that exhibit low Ti and REE and high Hf, U, and Th, and bright zones that exhibit high Ti and REE and low Hf, U, and Th.

Zircons from all three of the cumulate samples are mostly fairly bright in CL, and most of these grains have at least thin rims that are moderate to bright (Fig. 3). These cumulate samples often exhibit internal resorption surfaces identified by truncated zoning often associated with curved zone boundaries and embayments, particularly where bright rims or interior zones surround darker centers. Melt and mineral inclusions are most commonly found in these bright zones adjacent to resorption surfaces (Fig. 3). Nearly all the grains in the three leucogranite samples exhibit very dark rims, with rim thickness varying from thin (<30 μm) in the transitional sample, SML54Z to moderate to very thick (up to 60 μm) in the more silicic leucogranites, LGZ and SML49Z (Fig. 3). Most grains in all the leucogranite samples have medium to bright centers, although some grains in sample LGZ do have very dark centers. Online Resource 1 describes zircon zones in spots analyzed by SHRIMP-RG, corresponding geochemical and geochronologic data (where available), and calculated T_{TiZ}.

Hf, Ti, and T_{TiZ} in Zircon

Online Resource 1 provides a summary of Hf and trace element compositions of 171 analyses of 58 zircons from four samples from the Spirit Mountain granite. Data from two additional samples (98 analyses, 41 zircons) were reported in Claiborne et al. (2006a), and are not included in Online Resource 1, but are included in graphical representations of the data set. Zircons from the Spirit Mountain granite contain 6,900 to 16,700 ppm Hf (0.75–1.82 wt% HfO_2). Titanium and T_{TiZ} decrease and U and Th increase systematically with increasing Hf (Figs. 4, 5). The leucogranite samples have higher maximum Hf concentrations than cumulates (16,700 and 15,000 ppm, respectively), primarily from analyses of the ubiquitous dark rims, and span the entire range of Hf values for all samples (Fig. 4; Online Resource 1). Low Hf from leucogranite samples are primarily from grain centers. Cumulate interior and rim Hf concentrations overlap nearly completely in range (7,273–15,037 ppm and 7,847–14,711 ppm, respectively),

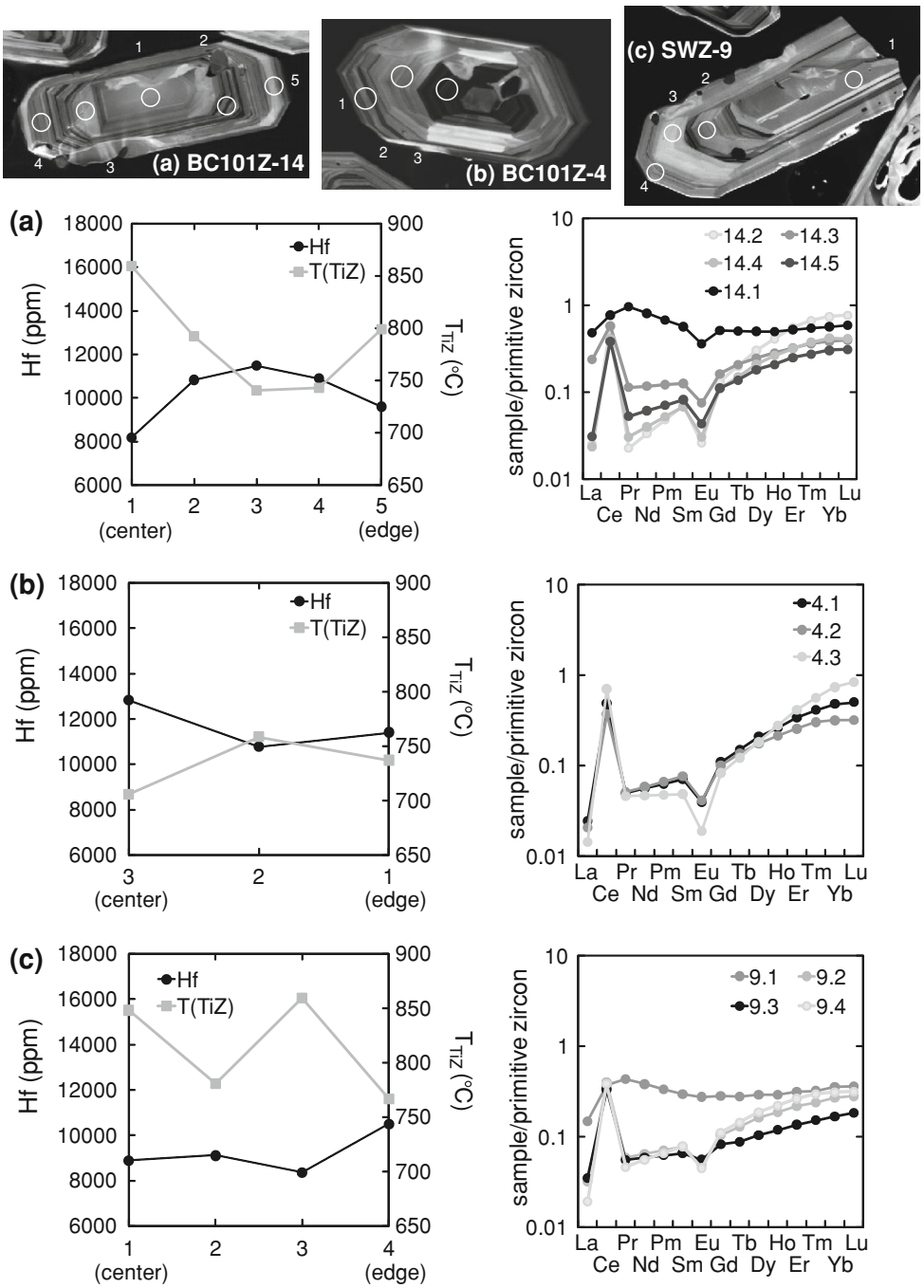

Fig. 3 Cathodoluminescence images of zircon grains from each sample showing zoning typical of that sample. **a–c** Zircons from cumulate samples BC101Z and SWZ. **d**, **e** Zircons from leucogranite samples SML-49Z and LGZ. *Circles* represent locations of SHRIMP-RG trace element analyses and are approximately 15 μm in diameter. Each grain is accompanied by corresponding Hf and Ti profiles and 'primitive' zircon normalized REE patterns (zircon REE were normalized to zircon analysis LGZ-8.1, which shows an especially unevolved composition, allowing clearer distinction of REE variations). *Shading* on REE lines increases in darkness with decreasing Hf, such that *black lines* represent the least fractionated, highest Ti analysis of any given grain

although the minimum Hf concentrations of cumulate rims is slightly higher than that of the interiors. Intragrain fluctuations in Hf are common and will be discussed further.

Titanium concentration and calculated temperatures from the Ti-in-zircon thermometer (T_{TiZ}) are inversely correlated with Hf; as Hf increases, Ti and T_{TiZ} decrease. Titanium concentrations in zircons from the Spirit Mountain batholith range from 3.3 to 36.1 ppm, yielding T_{TiZ} ranging from 680 to 925°C with similar variation within samples and up to 100°C variation within grains. Histograms of Ti concentration and resulting T_{TiZ} for each sample (Fig. 6) show that all six samples from both cumulates and leucogranite mainly yield temperatures between 700 and 850°C, with 33% of analyses showing temperatures greater than 800°C. Zircon analyses from cumulate samples yield no temperatures less than 700°C, and generally have a larger percentage of high calculated

Fig. 3 continued

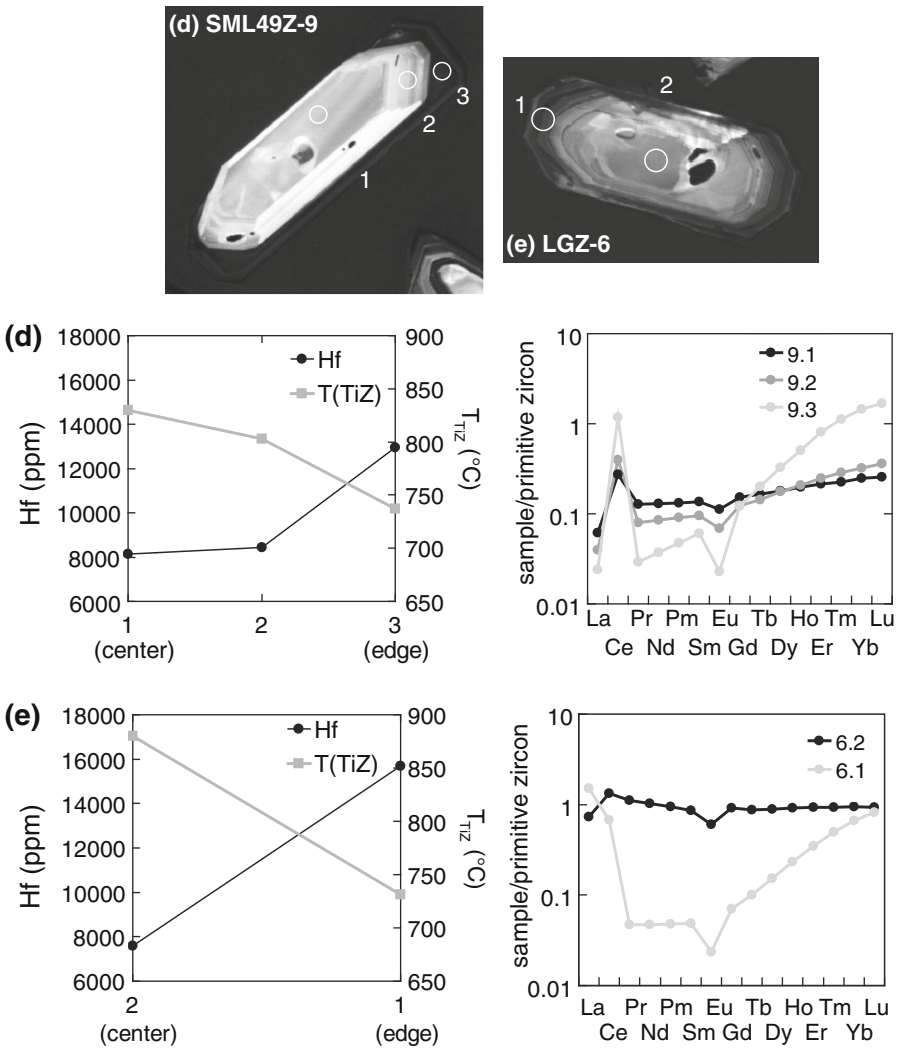

temperatures than the leucogranites. Unlike the other cumulate samples that exhibit a broad distribution of temperatures between 700 and 950°C, sample BC101Z has a fairly restricted range, with most temperatures between 700 and 800°C and only 15% of analyses above that. The transitional sample and both leucogranites samples have at least one analysis each below 700°C. The transitional sample is bimodal, with a peak population between 700 and 750°C and another between 800 and 850°C. Both leucogranites are distinctly unimodal, with a main temperature population between 700 and 750°C. The two leucogranite samples exhibit very different ranges, with analyses from LGZ yielding temperatures spanning the entire range up to 925°C, and sample SML49Z containing greater than 75% of its temperatures between 700 and 750°C, and no temperatures above 850°C.

The sample-to-sample variation in composition of zircon populations described above is relatively subtle, particularly between samples of similar lithology. In contrast, intragrain and grain-to-grain variability within each sample are striking. In some cases, the variability within single grains spans much of the compositional range of the entire sample suite. Individual zircon grains exhibit variation in T_{TiZ} and Hf (and U, Th, REE) corresponding to visible zones in CL images (Fig. 3). In grains from samples where several spots were analyzed, most exhibit fluctuations rather than monotonic change from core to rim. In grains where two or less spots were analyzed, patterns of variation are similar to those revealed more fully in grains with three or more analyzed spots. Zircons from cumulate sample SWZ have generally bright, high temperature, low Hf cores, surrounded by darker interior zones with lower T_{TiZ} and higher Hf which are then surrounded by bright, higher T_{TiZ}, low Hf rims 20–50 μm thick (Fig. 3). The other two cumulate samples are not as uniform in compositional zoning patterns. Both BC101Z and DSCG contain some zircons with moderately dark cores that exhibit low T_{TiZ} and high Hf and some grains that have bright cores with

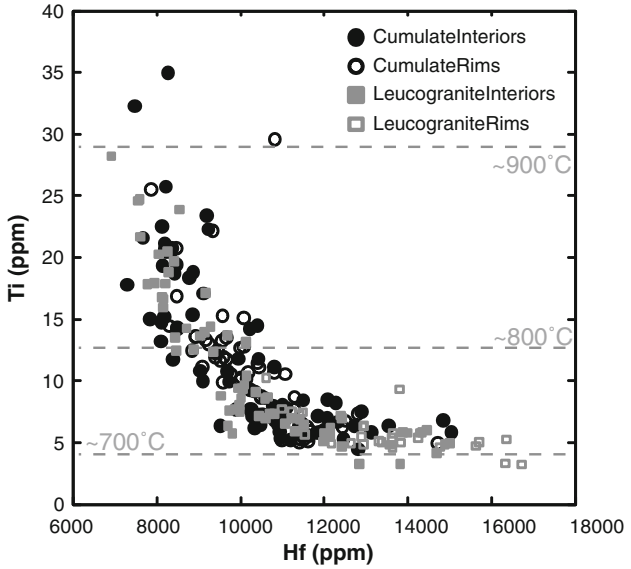

Fig. 4 Hafnium concentration versus Ti concentration in zircons. *Dashed lines* represent estimated temperatures for a given Ti concentration, calculated from the Ti-in-zircon thermometer (Ferry and Watson 2007) assuming $a_{TiO_2} = 0.7$ and $a_{SiO_2} = 1$

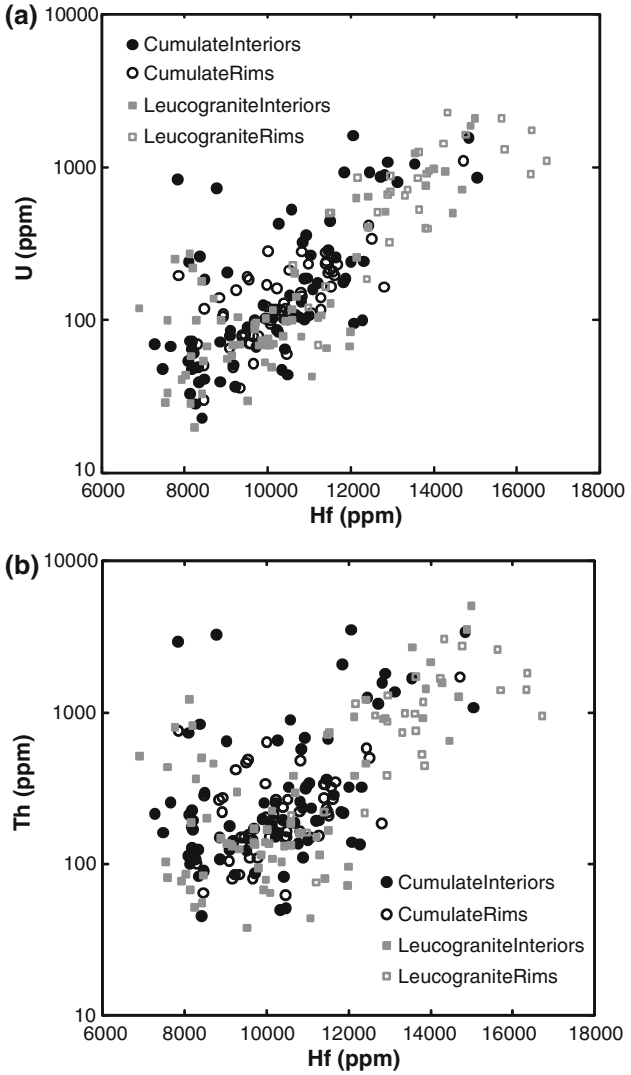

Fig. 5 **a** Hafnium concentration versus U concentration in zircons. **b** Hafnium concentration versus Th concentration in zircons

higher T_{TiZ} and lower Hf. Most zircons from both of these samples, however, do exhibit fluctuations in T_{TiZ} and Hf from core to rim of up to 100°C and 5,000 ppm Hf (Fig. 3).

Nearly all of the zircons from both leucogranite samples have thick (20–60 μm), very dark rims visible in CL images that are quite distinct from any cumulate sample and correspond to relatively low T_{TiZ} (680–750°C) and high Hf (10,500–17,500 ppm) (Fig. 3). The cores and interiors of grains from the two samples are more variable, however. All zircons analyzed from SML49Z exhibit general core to rim cooling and fractionation, with cores of T_{TiZ} between 725 and 835°C and 7,500–11,000 ppm Hf surrounded by the previously mentioned thick, "cool," fractionated rims (Fig. 3). Zircons from sample LGZ are more variable, some exhibiting low temperatures and high Hf throughout with core to rim cooling and fractionation, some with bright cores showing relatively high T_{TiZ} and low Hf, and some with dark interior zones with lower T_{TiZ} and higher Hf than either the core or rim (Fig. 3).

Because the interior and rim data for the transitional sample was nearly identical to the leucogranite interior and rim data, and it was so similar compositionally and mineralogically to the leucogranites, it is treated in geochemical plots and in remaining discussions as a leucogranite. The zircons in the transitional sample also all exhibit dark rims, although thinner than in the other leucogranites (1–30 μm), with very low temperatures and high Hf (680–730°C and 12,500–15,000 ppm, respectively). The cores of these zircons are mostly bright, with moderate to high T_{TiZ} and moderate to low Hf. A few cores are dark with low T_{TiZ} and high Hf. Many grains from this sample have a bright interior zone that has higher T_{TiZ} and lower Hf than either the core or rim (Fig. 3).

Uranium and thorium in zircon

Uranium varies from 20 to 4,750 ppm, with 80% of analyses between 20 and 300 ppm and only 3 above 2,300 ppm (Fig. 7a). Th varies from 40 to 23,300 ppm, with 70% of analyses between 40 and 400 ppm, and 4 above 3,500 ppm (Fig. 7b). Both U and Th remain fairly uniform and low at low Hf (less than 10,000 or 12,000 ppm Hf, respectively), then generally increase with increasing Hf (Fig. 5). Thorium/uranium is greater than 1, ranging from ~1 to ~4.5, with the most extreme enrichment in Th relative to U corresponding to low Hf and high T_{TiZ}

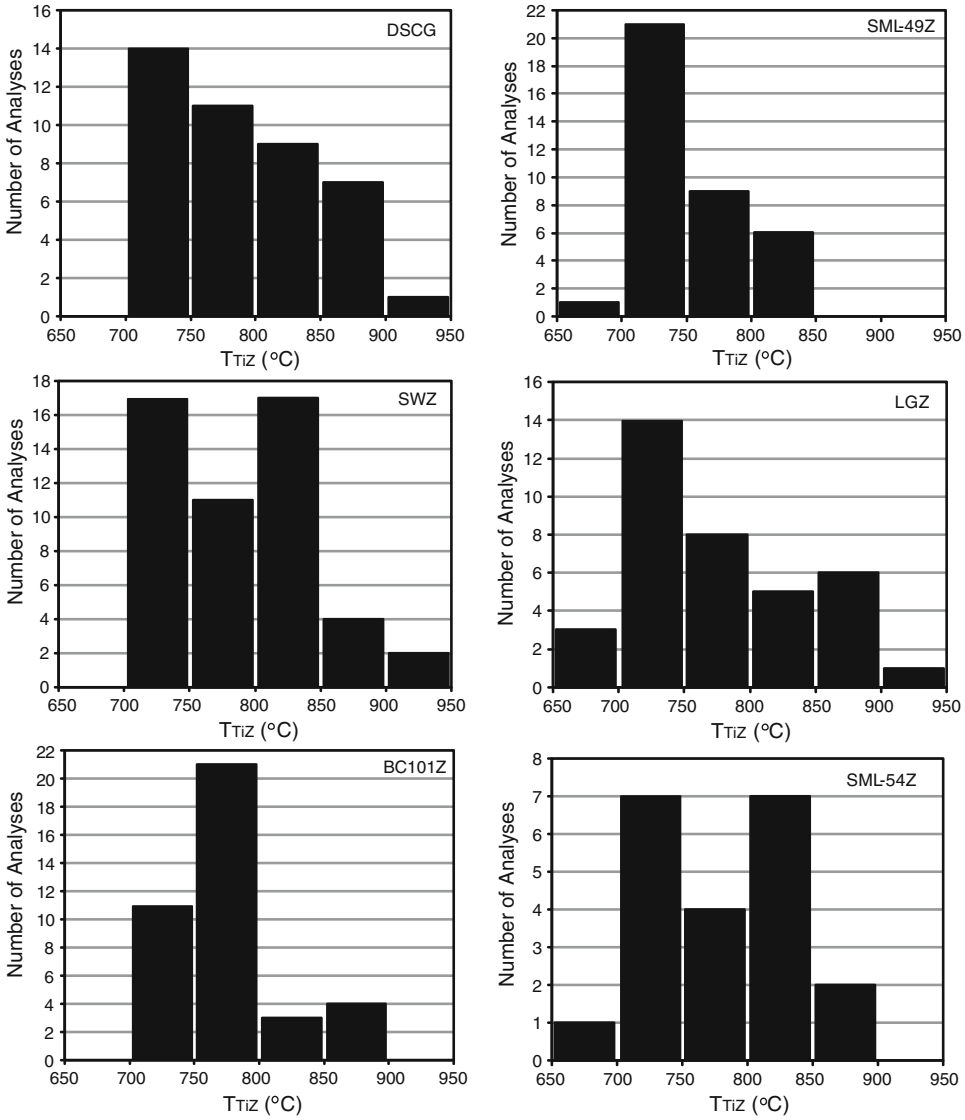

Fig. 6 *Histograms* showing distribution of temperatures from Ti-in-zircon thermometry for each sample

(Fig. 8a, b). The leucogranite samples have higher maximum U and Th than zircons from the cumulate samples. All leucogranite rims are in the upper ranges for both (greater than 100 ppm U and 200 ppm Th). The rims of the leucogranite samples have the highest U, while the interiors have the highest Th (approached by some cumulate analyses). Leucogranite rims have lower Th for the same U as leucogranite interiors or cumulate samples, apparently marking slightly different Th/U trends (Fig. 8a, b).

REE in zircon

The chondrite-normalized REE patterns of natural zircons are very strongly enriched in heavy REE relative to light REE and have positive Ce and negative Eu anomalies (Fig. 9). Within suites of related zircons, the similarities may be even stronger. These common characteristics dominate the appearance of chondrite-normalized patterns and mask meaningful variability. To reveal important differences among the Spirit Mountain zircon compositions, we normalize to the concentrations in a typical "primitive" (high T_{TiZ}, low Hf) zircon zone (Fig. 3). This reveals that like Hf, T_{TiZ}, Th, and U, REE concentrations and patterns in zircon vary significantly from sample to sample, from grain to grain within a sample, and even within individual grains. This enrichment in heavy REE relative to light REE increases with fractionation and lower T_{TiZ} (Figs. 3, 10a) resulting in variation in heavy REE such as Lu by a factor of 10 (Fig. 10b). Middle REE such as Sm and Gd vary by two orders of magnitude from 0.3 to 30 ppm, increasing with increasing T_{TiZ} and decreasing Hf (Fig. 10c). Light REE concentrations, exemplified by La, often show relative enrichment that we regard as highly unlikely for natural zircon (Fig. 3d, h, i). These high concentrations may

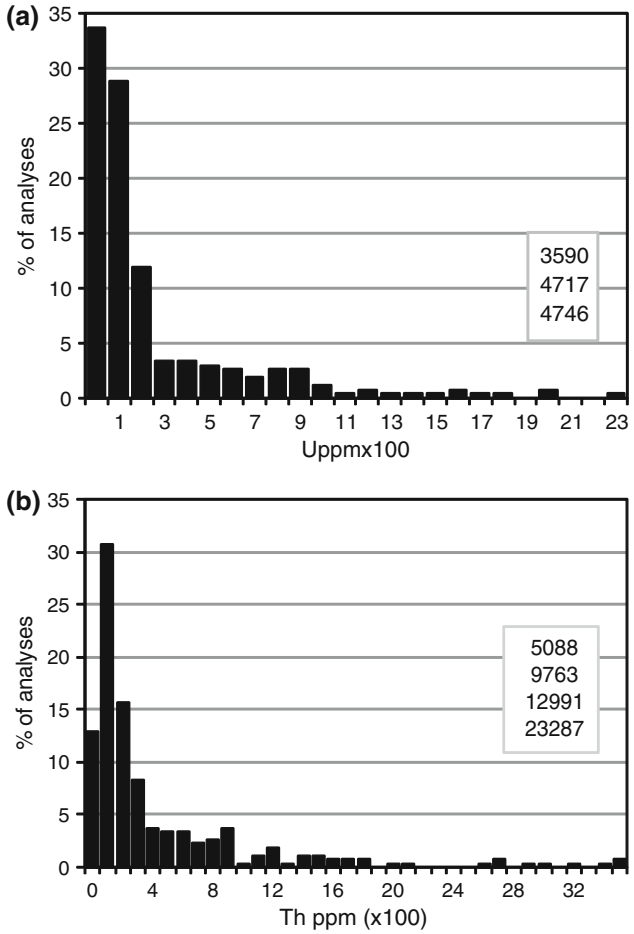

Fig. 7 Histograms showing distribution of **a** uranium concentrations and **b** thorium concentrations in zircons from all six samples. *Numbers* in *boxes* represent results that plot outside the scale of the *histograms*

be dominated by minute inclusions of light REE-rich mineral inclusions (e.g., allanite, chevkinite—both present in Spirit Mountain granites) or small melt inclusions. Any light REE-rich mineral or melt inclusion could potentially strongly influence the analyses of the naturally low concentration of light REE in zircon without significantly affecting the concentrations of the more abundant heavy REE, Hf, U, Th, and Ti. In analyses where presence of light REE-rich inclusions are not suspected, La concentrations vary by two orders of magnitude, from ~0.001 to 0.1 ppm (Online Resource 1). Primitive zircon-normalized REE patterns for fractionated samples commonly illustrate heavy REE enrichment and middle REE depletion, indicated by a steep negative slope between the heavy and middle REE and shallower or flat slope between the middle REE and light REE (Fig. 3b spot 4.3).

The zircons from the Spirit Mountain granite exhibit a negative Eu anomaly and positive Ce anomaly in chondrite-normalized REE plots (Fig. 9). The magnitude of the Eu anomaly increases with increasing fractionation and decreasing T_{TiZ} (Fig. 10d). Most of the change in the Eu anomaly is in the interiors, both cumulate and leucogranite. The maximum Eu/Eu* values, 0.4–0.5, are represented by five interior analyses, otherwise Eu/Eu* values below 0.4 are most characteristic of the maximum Eu/Eu* measured for these samples. The positive Ce anomaly also increases with increasing fractionation and decreasing T_{TiZ} (Fig. 10e). At high Hf the magnitude of the Ce anomaly increases sharply, primarily in the leucogranite rims, corresponding to increasing U, Th and heavy REE (Fig. 10e). The Ce concentration appears to correlate weakly with fractionation (Fig. 10f).

Comparison of the total 3+ ions in each analysis ($Sc^{3+} + Y^{3+} + REE^{3+}$) to P as a molar ratio reveals the ratio is nearly always greater than unity: that is, the substitution of 3+ cations for 4+ Zr is only partly charge-balanced by substitution of P^{5+} for Zr^{4+} ('xenotime substitution'). The amount of 3+ ions incorporated at any spot increases with P in a scattered, but grossly linear trend, and total 3+/P increases with increasing Hf and decreasing T_{TiZ}, with maxima defined by leucogranite rims (Fig. 11). The highest concentrations of P (ppm) and total 3+ ions are in spots with very low Hf and high T_{TiZ}.

Discussion

Ti-in-zircon thermometer

It has been suggested (Fu et al. 2008) that further application of the Ti-in-zircon thermometer in natural systems with careful consideration of petrologic context is necessary to determine whether Ti-in-zircon is a reliable indicator of temperature. This is particularly true considering that our data, along with other studies (Miller and Wooden 2004; Bacon and Lowenstern 2005; Walker et al. 2007; Miller et al. 2007a, b), suggest that it is common for zircons to finally reside in melt to which they are not cognate. This study, in which we can use the geochronology and trace element composition of the zircon along with extensive field observations and petrologic data, allows us to fit Ti-in-zircon temperatures into previously established zircon histories and test the thermometer.

All calculated Ti-in-zircon temperatures, including maxima and minima, are reasonable for felsic magmas and for zircon growth. A discussion of relationships between zircon saturation and calculated T_{TiZ} can be found in the following section on zircon growth. Calculated T_{TiZ} from zoned zircons document sequences of changing thermal environments during growth that were previously suggested by field, petrologic and geochronologic relations (Walker et al. 2007). These temperatures also correlate

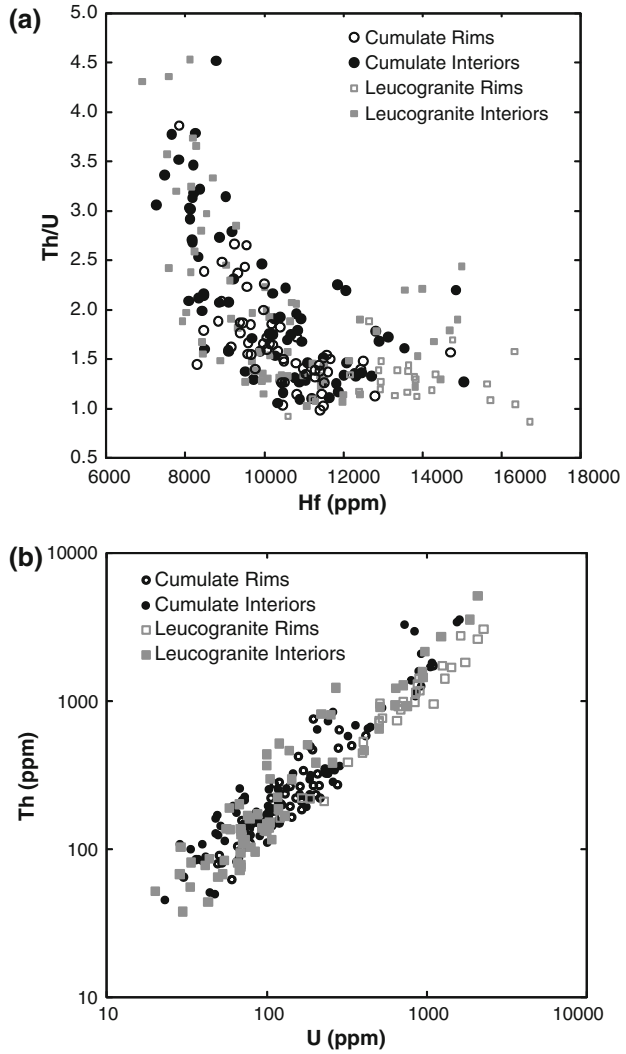

Fig. 8 Hafnium concentration versus Th/U from zircons

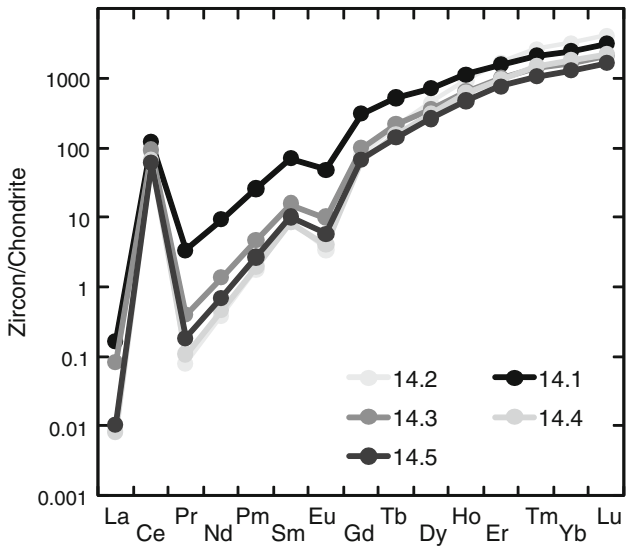

Fig. 9 Chondrite-normalized REE plot for sample BC101Z grain 14; corresponds to Fig. 3a

well with zircon trace element data that also support such a history. The higher temperatures and common fluctuations recorded in zircons from the cumulate samples and the ubiquitous low temperature, fractionated rims on zircons in the leucogranites support at least the relative validity of the calculated temperature variations. Since the Ti-in-zircon record appears to correlate with all the other records, we feel confident that our assumptions were in fact, reasonable and the calculated temperatures are useful.

The ubiquity of sphene in all samples indicates relatively high a_{TiO_2}. If our assumed a_{TiO_2} (0.7) is either an over or underestimate, the relative variations in temperature recorded by the zoned zircons remain intact and the resulting conclusions are robust. Ferry and Watson (2007) argue that a_{TiO_2} and a_{SiO_2} will likely vary together and therefore counterbalance their respective effects on the thermometer. As we have used a fixed value for both and calculations result in temperatures and relative temperatures that are reasonable in field, petrologic, and geochemical context, we again feel confident that these calculated temperatures are useful.

In addition to the issue of changing or unknown activity of TiO_2 and SiO_2, potential problems that have been associated with the thermometer include possible errors in calibration, pressure dependence (Tomkins et al. 2007; Anderson et al. 2007; Ferriss et al. 2008), subsolidus resetting of Ti composition, non-Henry's Law substitution of Ti into the zircon structure (Fu et al. 2008), and disequilibrium crystallization from melts (Fu et al. 2008). We argue that sufficient experimental (Watson and Harrison 2005; Watson et al. 2006; Ferry and Watson 2007; Hayden and Watson 2007) and natural studies have been performed in field, geochemical and petrologic context that show well constrained and reasonable results (Claiborne et al. 2006a; Reid et al. 2006; Vazquez et al. 2006; Reid and Vazquez 2006; Bea et al. 2007; Bromley et al. 2007; Miller et al. 2007b; Leslie et al. 2007; Bolhar et al. 2008; Hiess et al. 2008) that calibration of the model apparently does not produce substantial error. Pressure dependence of the thermometer if applied to the Spirit Mountain batholith could result in temperatures that are tens of degrees lower than those reported herein (Ferriss et al. 2008; Ferry and Watson 2007), but does not affect our conclusions regarding relative temperature changes or move the temperatures out of a range reasonable for felsic magmas. CL images show magmatic textures for all grains, with no evidence for recrystallization. The retention of distinct trace element zoning tracked by our SHRIMP data indicates no diffusional, sub-solidus re-equilibration of Ti has occurred. Finally, at the low Ti concentrations under

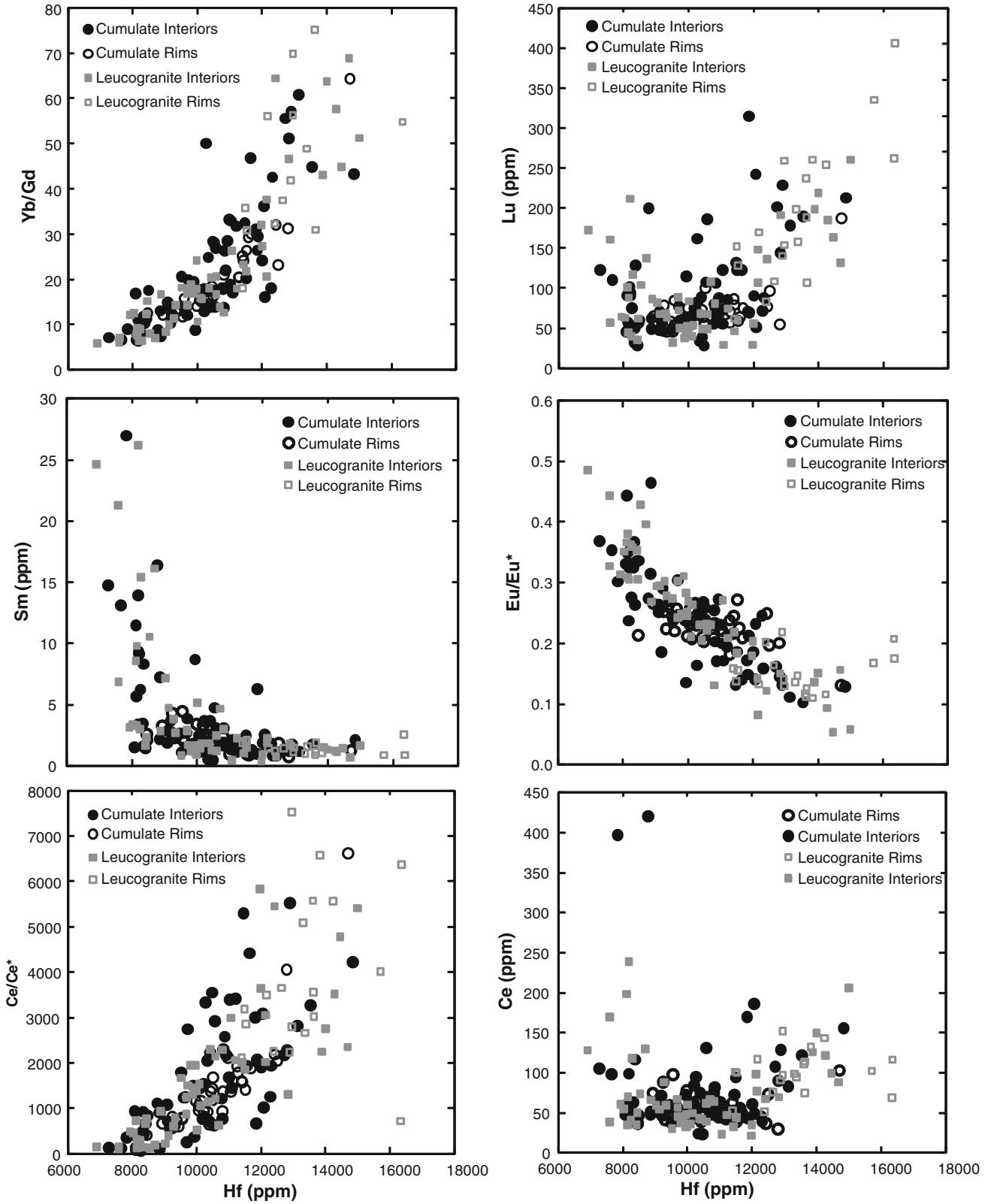

Fig. 10 **a** Hafnium concentrations versus Y/Gd in zircons illustrates variation in heavy REE versus light REE with fractionation. **b** Hafnium concentrations versus Lu concentrations in zircons. **c** Hafnium concentrations versus Sm concentrations in zircons. **d** Hafnium concentrations versus Eu/Eu*, or Eu anomaly, in zircons. **e** Hafnium concentrations versus Ce/Ce*, or Ce anomaly, in zircons. **f** Hafnium concentrations versus Ce concentrations in zircons

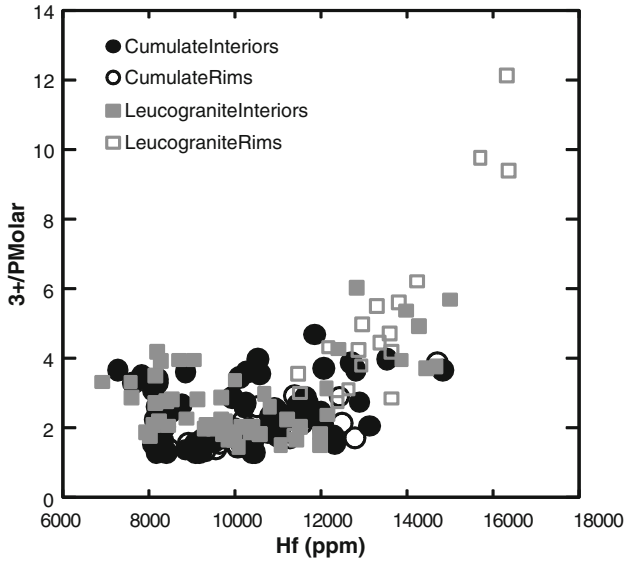

Fig. 11 Hafnium concentrations versus (the sum of all 3+ ions)/*P* to illustrate departure from the 'xenotime' substitution

consideration, it is reasonable to assume Henry's Law substitution and neglect potential kinetic effects. Since our data do fit well with previously established petrologic and geochronologic models and with other geochemical indicators, we argue that these assumptions are reasonable and well founded in this case. If for other studies, the resultant temperatures do not make petrologic sense, then it may be necessary to reconsider one or more of these assumptions for each specific case.

Zircon growth and dissolution

A comparison of calculated zircon saturation temperatures with T_{TiZ} for the putative 'primary' magma represented by sample BGZ and the 'crystal-poor fractionated melt' represented by sample LGZ reveals some discrepancy. The highest Ti-in-zircon temperatures, from cumulate samples, are ~140°C higher than the calculated saturation temperature for what is assumed to be the batholith input composition. Only two T_{TiZ} from the rims of leucogranites that are assumed to have grown directly from segregated melt are appreciably higher (~50°C) than the zircon saturation temperature for crystal-poor LGZ, and one of these rims appears to be generally more 'primitive' and therefore we would expect a higher T_{TiZ}. Harrison et al. (2007) found that in plutonic rocks, it is common for ~50% of T_{TiZ} to be greater than calculated zircon saturation temperatures. Normal crystallization of zircon-undersaturated melt will increase its zircon saturation temperature, as Zr concentration and '*M*' value in the remaining melt increases. Since none of these natural samples, particularly the cumulate samples, was likely devoid of crystals when zircon began growing, it is expected that these zircon saturation temperatures calculated from bulk rock compositions will be underestimates. Plausibly, unusually high T_{TiZ} zones could reflect growth in Zr-rich melt pockets formed during reheating of zircon-rich cumulate mush. Alternatively, they might be derived from grains that grew at elevated *T* in fractionated mafic magma, perhaps redistributed by disaggregation of enclaves.

Zircons from Spirit Mountain batholith do not exhibit a monotonic decrease in T_{TiZ} following the onset of crystallization, as would be predicted by simple crystallization and cooling (Harrison et al. 2007). Rather, the complexity in zoning suggests that the zircon population of each sample grew either in a complex magmatic environment with fluctuating conditions or during separate, repeated episodes of crystallization. Both scenarios are supported by ubiquitous resorption surfaces and embayments within zircon grains that suggest zircon-saturated magmas were repeatedly rejuvenated or mixed with hotter, zircon-undersaturated magmas. These surfaces are commonly surrounded by bright zones with higher T_{TiZ}, suggesting that the rejuvenation or mixing allowed zircon to saturate at a higher temperature than previously. In order to achieve zircon growth at these higher temperatures, the Zr concentration in the melt must have increased (along with the other elements that comprise the '*M*' factor). This could occur as rejuvenation dissolves zircon-rich cumulate, increasing the temperature required for saturation to temperatures that would normally result in total zircon dissolution (>800°C). Some change in zircon saturation temperature might also be expected with introduction of a new magma with a different composition, although the large volumes of chemically, modally similar granite with a large age range (Walker et al. 2007) suggests that the composition of input magmas, with the exception of apparently low-volume mafic magma, were likely very similar throughout the lifetime of the batholith. Some bright, high T_{TiZ} zones surround darker cooler zones with no evidence of resorption. This could be attributable to buffering of zircon grains as inclusions in phenocrysts during periods of rejuvenation and dissolution, which would be an important consideration in interpreting any zircon data. These un-resorbed zircon grains apparently only contacted the higher temperature melt once the melt had re-saturated in zircon at the higher temperature. Alternatively, cores of cumulate zircons could represent grains injected into the system with input magmas, and could have grown at greater depth.

Ideally, we would like to correlate age and trace elements, including Hf, Ti and T_{TiZ}, in order to discuss timescales of growth and dissolution processes as well as a specific chronology of events during the assembly of the batholith and the resulting timescales. However, due to the relatively large errors on the geochronologic data, inherent

to U–Pb systematics in zircons of this age, no significant correlations can be made.

Composition of igneous zircon: implications for magma evolution

As there is also no evidence of re-equilibration or recrystallization, we assume the zircon geochemistry is indicative of its incorporation of constituents at the time of growth. Incorporation of dispersed elements into zircon should directly reflect melt composition according to an appropriate Henry's Law partition coefficient. However, partition coefficients for zircon are the subject of ongoing research and debate, in part because they are sensitive to changes in melt composition, oxygen fugacity and water content; furthermore, kinetic effects including boundary layer formation and disequilibrium crystallization can influence uptake of elements and effective partition coefficients (Kds) (Watson 1980, 1996; Hanchar and van Westrenen 2007). Because of this, and due to difficulties in attaining useful experimental data, Kds for REE incorporation during zircon growth from felsic melts are highly variable from study to study and may be unreliable (Luo and Ayers 2009). Partition coefficients for elements in higher abundance in zircon such as U and Th are more straightforward and are utilized below.

Systematic variation in trace element composition with temperature (T_{TiZ}) and degree of fractionation (as indicated by Hf) and covariance of T_{TiZ} with Hf that correlates with sample bulk rock chemistry and petrology, geochronology, and field relations together suggest that the composition of these zircons generally corresponds to real variation in melt composition. The close fit of our zircon data to petrologic context gives us confidence that zircon composition can be relied on to determine complexity in magmatic history and track evolution and fluctuations in magma temperature and composition, in spite of uncertainties in specific Kds. Certainly the general pattern of partition coefficient change is correct for zircon which means that the zircon composition can be used to generally interpret gross changes in magma composition (i.e., the high Yb/Gd ratios in zircon rims must reflect a melt pattern with flat or even negative slope for the heavy REE).

Relatively high Th/U (>1 with high maxima) is a common characteristic of zircon from the Tertiary igneous rocks of the Mojave terrane, reflecting high magmatic Th/U that appears to be related to the regional lithosphere, although Th/U of these zircons is especially high. The ratio is especially high (up to 4.5) in zones that grew from higher temperature, less evolved melt, and drops rapidly with decreasing Hf and T_{TiZ}, leveling off at $\sim$1.5 in zones that exhibit a cooler, evolved signature. These "cool" zones are richest in both U and Th. The initial sharp drop in this ratio is common in zircon, probably reflecting greater incompatibility of U than Th with crystallizing assemblage, and suggesting a lack of early accessory mineral crystallization, as coeval crystallization of sphene, allanite and/or chevkinite would result in a decrease in both elements. More puzzling is the leveling off of the ratio in evolved portions of the zircon with high U and Th, suggesting that the two elements were both highly and equally incompatible with the most evolved mineral assemblages.

Published zircon/melt partition coefficients for U and Th vary by well over an order of magnitude (e.g., Mahood and Hildreth 1983; La Tourrette et al. 1991; Bea et al. 1994; Rubatto and Hermann 2007; cf. Blundy and Wood 2003; Charlier and Zellmer 2000; Wilson et al. 2006). These experimental and empirical studies appear to show a systematic increase in Kd with falling temperature, with values reaching 200–400 for U and 50–100 for Th at temperatures below 800°C. Using these Kds and evolved zircon compositions from leucogranite samples, concentrations of U and Th in the more evolved melts should be $\sim$4 and $\sim$20 ppm, respectively. This compares with typical U and Th concentrations of $\sim$2–8 and 17–68 ppm in fine-grained leucogranites that are considered to approximate the compositions of crystal-poor segregated melts from which these evolved zircon zones grew. Taking the fine-grained granites (sample BGZ) as representative of the input magma that formed the batholith ($\sim$1.5 ppm U, $\sim$14 ppm Th), both the U-enriched zircon zones and the whole-rock leucogranite U concentrations appear to require at least 80% fractional crystallization to form the typical highly evolved melts and $\sim$90% to form the most extreme compositions. These rim zones thus have quite reasonable compositions. Common concentrations of U and Th of $\sim$50 and 150 ppm, respectively, found in zircons from all samples may represent growth following initial zircon saturation; using likely partition coefficients for $T = 800$–900°C of greater than 50 and 15 (see references above), these values suggest melt concentrations less than 1 and 10 ppm, respectively, similar to the measured concentrations of the input magma.

Miller and Wooden (2004) and Bindeman et al. (2008) suggest that melts with the highest U and Th concentrations indicated by zircon compositions from rhyolites that they studied (Coso, California, and Yellowstone) may reflect extreme fractional crystallization (>95%) and represent late stage, uneruptible melt, and thus that zircon with this composition documents growth in a specifically plutonic environment. Miller and Wooden (2004) point out that these late melts would be restricted by their low volumes and Zr concentrations to produce a very limited volume of zircon. It appears that rims on Spirit Mountain leucogranite zircons reflect similar, but somewhat less extreme, fractionation and an appropriately larger volume.

REE compositions of zircons in this study are in a very general sense typical for igneous zircon (Hoskin and Schaltegger 2003) in that they are highly enriched in the heaviest REE, with enrichment decreasing systematically with decreasing atomic number. The exceptions to this regular pattern of increasing enrichment with atomic number, as with most zircons from granitic compositions, are positive Ce and negative Eu anomalies. Sharp increase in heavy REE enrichment and light REE depletion with fractionation are likely a function of extreme variation (increase or decrease, respectively) of concentrations of those elements in the melt as the melt composition becomes highly fractionated. Variations in zircon REE patterns probably reflect coeval crystallization of accessory minerals in which REE behave compatibly (i.e., sphene, allanite and chevkinite). Growth of these minerals modifies REE patterns in the melt, and therefore in the growing zircon. The steeply positive middle to heavy REE accompanied by relatively flat light to middle REE visible in primitive zircon-normalized REE plots document a relative middle REE depletion and may indicate zircon growth coeval with sphene, which preferentially incorporates the middle REE (e.g., Glazner et al. 2008).

The modest Eu/Eu* values observed here suggest parental magmas that either had experienced significant feldspar fractionation before zircon reached saturation or had an initial negative Eu anomaly as the result of being derived from a feldspar-rich source. The variation in the Eu anomaly for rims from both cumulates and leucogranites is small, suggesting that the Eu anomaly is being somewhat buffered in the rims, likely due to growth of coeval accessory minerals, including sphene. As expected, the leucogranite rims have a more negative anomaly than the cumulate rims, supporting the more fractionated character of the leucogranite melts. As with other elements, the overlap of Eu/Eu* cumulate interior analyses and leucogranite rim analyses suggests that parts of the cumulate zircons did grow from melts as fractionated as those from which the leucogranite rims grew, but in general were in equilibrium with a less fractionated melt for their final stage of growth. This observation is consistent with the model for the extraction of the leucogranite melts from what became cumulates, and that the cumulates are the product of repeated injections of less fractionated magma.

The ubiquitous positive Ce anomaly is the result of compatibility of Ce^{4+} with zircon, a consequence of its similar ionic radius and identical charge to Zr^{4+}. This contrasts to the trivalent light REE, which are mismatched with Zr in both charge and radius and, compared to other REE, are extremely incompatible with zircon. It has been suggested that the magnitude of the anomaly is controlled by the oxygen fugacity of the magma and that it thus can be used to provide information on the fO_2. However, while the Ce anomaly in the zircons varies by a factor of more than 50, we see no independent evidence of changes in melt fO_2. We argue that while the Ce^{+3}/Ce^{+4} of the melt may in part reflect the fO_2 (Hoskin and Schaltegger 2003), partitioning of Ce^{3+} and Ce^{+4} among coexisting phases may be more influential. The increasing Ce anomaly in zircon may be explained by highly compatible behavior of trivalent LREE during growth of other accessory minerals (allanite, chevkinite, sphene, and apatite), but relatively incompatible behavior of Ce^{4+}, which is likely compatible only with zircon and therefore would not decrease as much as other LREE and might actually increase in concentration as crystallization progresses. This behavior would be analogous to that demonstrated for Eu^{2+}/Eu^{3+} in clinopyroxene in highly fractionated melts (Ayers 1993).

Spirit Mountain batholith: construction and evolution of a large silicic system

The major and trace element geochemistry of zircons from the Spirit Mountain batholith appears to record the same history of protracted accumulation, repeated reheating and rejuvenation of zones within crystal mushes and episodic fractionation and melt segregation events, that is suggested by the petrology, field relations and U–Pb geochronology. Zircons from cumulate samples appear to have grown from relatively high temperature, less evolved melts (either in the cumulate pile or at some greater depth) and the ubiquitous evidence for resorption followed by growth at higher temperatures attests to their presence in a melt experiencing repeated inputs of new, hot magma. Zircons from leucogranites often contain cores that share this history with the cumulate zircons, representing grains that were carried along with the extracted, crystal-poor melt during segregation events (Claiborne et al. 2006a, b). Rims on all leucogranite grains and cores of some appear to have grown entirely from highly evolved, cooler melt, presumably following the segregation event and injection of the extracted melt into the roof zone.

The extreme melt evolution recorded in some zircons requires significant crystallization and could potentially be used as an indicator of plutonic or near-solid conditions that are past the rheological limits for eruptibility or melt extraction (Bindeman et al. 2008; Miller and Wooden 2004; Ayers 1993). Zircons from the leucogranite samples from the Spirit Mountain batholith do attain these extreme compositions, particularly in rims and do record crystallization in highly evolved melts requiring significant crystallization. However, both cores and rims of grains in the leucogranite record this, suggesting that from the time of interstitial melt extraction and throughout the entirety of new zircon growth, these conditions prevailed. This extracted melt was definitively below the eruptible

rheological limit at the time of extraction and presumably for some time after. Similarly, no zircons from the cumulate samples that were presumably growing both prior to and after reaching the rheological limit show this signature, though they are irrefutably plutonic in nature. Although extreme composition zircons must have grown from highly evolved melts that had at some point undergone significant crystallization, considering this set of plutonic data along with the unreliability of zircon/trace element partition coefficients, it does not appear reasonable to use zircon compositions to divide definitively *plutonic* from definitively *volcanic* zircons.

Constraining the timescales of the magmatic processes through which a large magma body like the Spirit Mountain batholith accumulates and evolves are essential to a better understanding of these processes. Zircon growth rates are poorly understood, but age analyses of cores and rims on individual grains suggest that individual grains record events hundreds of thousands of years apart. We cannot definitively determine whether these grains record extended histories through constant slow growth punctuated by periods of dissolution, or record episodes of growth hundreds of thousands of years apart. With U–Pb SHRIMP dating of zircons, errors are often on the order of hundreds of thousands of years, and these do not allow us to resolve the timing of heating or melt extraction events, although the complexity of the system over its lifetime appears irrefutable. As established by Walker et al. (2007), it is apparent that the Spirit Mountain batholith did accumulate over 2 million years and that repeated episodes of intrusion and heating followed by crystallization and melt segregation throughout that history built the body into its current form.

Conclusions

Hafnium, U and Th, and REE content of zoned zircons from the Spirit Mountain batholith correlate with calculated temperatures from the Ti-in-zircon thermometer as well as with field and petrologic evidence of rejuvenation of crystal mush and melt extraction events during the 2-million year accumulation of this patchwork batholith. While the timescales of specific events cannot be resolved, it is apparent that multiple rejuvenation and reheating events affected zircon grains within individual samples and that each sample contains grains that experienced different histories. These zircons document changes in the trace element budget of the magmas, potentially recording crystallization of other phases that exert control over this budget, such as sphene, allanite and chevkinite, and tracking general evolution of the magma with reheating, crystallization and segregation events. These zircons therefore tell a story of a large body with melt fraction and composition varying in both time and space, recycling these refractory zircon crystals during repeated episodes of intrusion, rejuvenation and interstitial melt extraction.

Acknowledgments This work was supported by National Science Foundation Grants EAR-0409876 and EAR-0107094. Frank K. Mazdab was instrumental in developing methods for analysis of trace elements in zircon using the SHRIMP-RG that we used in this study. We would like to thank BJ Walker for spending time in the field and in discussion working with us on puzzling out the history of the Spirit Mountain batholith. Discussions with Jonathan Miller regarding behavior of zircon in magmatic systems contributed to this work. Discussions with Ashley Bromley, Guil Gualda, Mark Ghiorso and Bruce Watson contributed to our understanding of a_{TiO_2} and its influence on the Ti-in-zircon thermometer. Thanks to David Hawkins and an anonymous reviewer for suggestions that improved this manuscript.

References

Ahrens LH, Erlank AJ (1969) Hafnium. In: Wedepohl KH (ed) Handbook of Geochemistry, 2–5, sections B-O. Springer, Berlin

Anderson BE, Essene EJ, Becker U (2007) Ti substitution in zircon. Geochim Cosmochim Acta 71:A27

Ayers JC (1993) Partitioning and mass-balance relations in lherzolites. Chem Geol 107:19–27

Bachmann O, Bergantz GW (2004) On the origin of crystal-poor rhyolites: extracted from batholithic crystal mushes. J Petrol 45:1565–1582

Bacon CA, Lowenstern JB (2005) Late Pleistocene granodiorite source for recycled phenocrysts in rhyodacite lava at Crater Lake, Oregon. Earth Planet Sci Lett 233:277–293

Bea F, Pereira MD, Stroh A (1994) Mineral/leucosome trace element partitioning in a peraluminous migmatite (a laser ablation-ICP-MS study). Chem Geol 117:291–312

Bea F, Montero P, Ortega M (2006) A LA-ICPMS evaluation of Zr reservoirs in common crustal rocks: implications for Zr and Hf geochemistry and zircon-forming processes. Can Mineral 44:693–714

Bea F, Montero P, Gonzalez-Lodiero F, Talavera C (2007) Zircon inheritance reveals exceptionally fast crustal magma generation processes in Central Iberia during the Cambro-Ordovician. J Petrol 48:2327–2339

Belousova EA, Griffin WL, O'Reilly SY, Fisher NI (2002) Igneous zircon: trace element composition as an indicator of source rock type. Contrib Mineral Petrol 143:602–622

Bindeman IN, Schmitt AK, Valley JW (2006) U/Pb zircon geochronology of silicic tuffs from the Timber Mountain/Oasis Valley caldera complex, Nevada: rapid generation of large volume magmas by shallow-level remelting. Contrib Mineral Petrol 152:649–665

Bindeman IN, Fu B, Kita NT, Valley JW (2008) Origin and evolution of silicic magmatism at Tellowstone based on ion microprobe analysis and isotopically zoned zircons. J Petrol 49:163–193

Blundy J, Wood B (2003) Partitioning of trace elements between crystals and melts. Earth Planet Sci Lett 210:383–397

Bolhar R, Weaver SD, Palin JM, Cole JW, Paterson LA (2008) Systematics of zircon crystallization in the Cretaceous Separation Point suite, New Zealand, using U/Pb isotopes, REE and Ti geothermometry. Contrib Mineral Petrol 156:133–160

Bromley SA, Miller CF, Claiborne LL, Wooden JL, Mazdab FK (2007) Record of hybridization preserved in zircon, Aztec Wash Pluton, NV. Eos Trans AGU 88:V51C-0705

Brown SJA, Fletcher IR (1999) SHRIMP U-Pb dating of the pre-eruption growth history of zircons from the 340 ka Whakamaru Ignimbrite, New Zealand: Evidence for > 250 k.y. magma residence times. Geol 27:1035–1038

Charlier B, Zellmer G (2000) Some remarks on U–Th mineral ages from igneous rocks with prolonged crystallization histories. Earth Planet Sci Lett 183:457–469

Charlier BLA, Wilson CJN, Lowenstern JB, Blake S, Van Calsteren PW, Davidson JP (2005) Magma generation et al large, hyperactive silicic volcano (Taupo, New Zealand) revealed by U–Th and U–Pb systematics in zircons. J Petrol 46:3–32

Cherniak DJ, Watson EB (2003) Diffusion in zircon. In: Hanchar JM, Hoskin PWO (eds) Zircon, reviews in mineralogy and geochemistry, vol 53. Mineralogical Society of America, Washington, pp 113–144

Cherniak DJ, Hanchar JM, Watson EB (1997a) Diffusion of tetravalent cations in zircon. Contrib Mineral Petrol 127:383–390

Cherniak DJ, Hanchar JM, Watson EB (1997b) Rare-earth diffusion in zircon. Chem Geol 134:289–301

Claiborne LL, Miller CF, Walker BA, Wooden JL, Mazdab FK, Bea F (2006a) Tracking magmatic processes through Zr/Hf rations in rocks and Hf and Ti zoning in zircons: An example from the Spirit Mountain batholith, Nevada. Mineral Mag 70:517–543

Claiborne LL, Furbish DJ, Miller CF (2006b) Determining mechanics of segregating small crystals from melt using modeling and SHRIMP-RG trace element analysis of zircons: An example from the Spirit Mountain batholith, Nevada. Eos Trans AGU 87:V54B-02

Coleman DS, Gray W, Glazner AF (2004) Rethinking the emplacement and evolution of zoned plutons: Geochronologic evidence for incremental assembly of the Tuolumne Intrusive Suite, California. Geol 32:433–436

Davidson JP, Morgan DJ, Charlier BLA (2007) Isotopic microsampling of magmatic rocks. Elements 3:253–259

Davies GR, Halliday AN, Mahood GA, Hall CM (1994) Isotopic constrains on the production-rates, crystallization histories and residence times of pre-caldera silicic magmas, Long Valley, California. Earth Planet Sci Lett 125:17–37

Eichelberger JC, Izbekov PE (2000) Eruption of andesite triggered by dyke injection; contrasting cases at Karymsky Volcano, Kamchatka and Mt Katmai, Alaska. Philos Trans R Soc Lond 358:1465–1485

Faulds JE, Geissman JW, Shafiqullah M (1992) Implications of paleomagnetic data on Miocene extension near a major accommodation zone in the Basin and Range province, northwestern Arizona and southern Nevada. Tectonics 11:204–227

Faulds JE, Feuerbach DL, Reagan MK, Metcalf RV, Gans P, Walker JD (1995) The Mount Perkins Block, northwestern Arizona: an exposed cross section of an evolving, pre-extensional to synextensional magmatic system. J Geophys Res Solid Earth Planet 100:15249–15266

Ferriss EDA, Essene EJ, Becker U (2008) Computational study of the effect of pressure on the Ti-in-zircon thermometer. Eur J Mineral 20:745–755

Ferry JM, Watson EB (2007) New thermodynamic models and revised calibrations for the Ti-in-zircon and Zr-in-rutile thermometers. Contrib Mineral Petrol 154:429–437

Finch RJ, Hanchar JM (2003) Structure and chemistry of zircon and zircon-group minerals. In: Hanchar JM, Hoskin PWO (eds) Zircon, reviews in mineralogy and geochemistry, vol 53. Mineralogical Society of America, Washington, pp 1–26

Fowler A, Prokoph A, Stern R, Dupuis C (2002) Organization of oscillatory zoning in zircon: analysis, scaling, geochemistry, and model of a zircon from Kipawa, Quebec, Canada. Geochim Cosmochim Acta 66:311–328

Fu B, Page FZ, Cavosie AJ, Fournelle J, Kita NK, Lackey JS, Wilde SA, Valley JW (2008) Ti-in-zircon thermometry: applications and limitations. Contrib Mineral Petrol 156:197–215

Gans PB, Bohrson WA (1998) Suppression of volcanism during rapid extension in the Basin and Range province, United States. Science 279:66–68

Glazner AF, Bartley JM, Coleman DS, Gray W, Taylor RZ (2004) Are plutons assembled over millions of years by amalgamation from small magma chambers. GSA Today 14:4–11

Glazner AF, Coleman DS, Bartley JM (2008) The tenuous connection between high-silica rhyolites and granodiorite plutons. Geology 36:183–186

Hanchar JM, Miller CF (1993) Zircon zonation patterns as revealed by cathodoluminescence and backscattered electron images: implications for interpretation of complex crustal histories. Chem Geol 110:1–13

Hanchar JM, van Westrenen W (2007) Rare earth element behavior in zircon-melt systems. Elements 3:37–42

Hanchar JM, Watson EB (2003) Zircon saturation thermometry. In: Hanchar JM, Hoskin PWO (eds) Zircon, reviews in mineralogy and geochemistry, vol 53. Mineralogical Society of America, Washington, pp 89–112

Hanchar JM, Finch RJ, Hoskin PWO, Watson EB, Cherniak DJ, Mariano AN (2001) Rare earth elements in synthetic zircon: part 1. Synthesis, and rare earth element and phosphorus doping. Am Mineral 86:667–680

Harley SL, Kelly NM (2007) Zircon: tiny but timely. Elements 3:13–18

Harper BE, Miller CF, Koteas GC, Cates NL, Wiebe RA, Lazzareschi DS, Cribb JW (2004) Granites, dynamic magma chamber processes and pluton construction: the Aztec Wash pluton, Eldorado Mountains, Nevada, USA. Trans R Soc Edinb Earth Sci 95:277–295

Harrison TM, Watson EB (1983) Kinetics of zircon dissolution and zirconium diffusion in granitic melts of variable water content. Contrib Mineral Petrol 84:67–72

Harrison TM, Watson EB, Aikman AB (2007) Temperature spectra of zircon crystallization in plutonic rocks. Geology 35:368–635

Hayden LA, Watson EB (2007) Rutile saturation in hydrous silicate melts and its bearing on Ti-thermometry of quartz and zircon. Earth Planet Sci Lett 258:561–568

Heaman LM, Bowins R, Crocket JH (1990) The chemical composition of igneous zircon suites: implications for geochemical tracer studies. Geochim Cosmochim Acta 54:1597–1607

Hiess J, Nutman AP, Bennett VC, Holden P (2008) Ti-in-zircon thermometry applied to contrasting Archean metamorphic and igneous systems. Chem Geol 247:323–388

Hildreth W (2004) Volcanological perspectives on Long Valley, Mammoth Mountain, and Mono Craters: several contiguous but discrete systems. J Volcanol Geotherm Res 136:169–198

Hopson CA, Gans PB, Baer E, Blythe AE, Calvert A, Pinnow J (1994) Spirit Mountain Pluton, southern Nevada; a progress report. Geol Soc Am Abstr Program 26:60

Hoskin PWO (2000) Patterns of chaos: fractal statistics and the oscillatory chemistry of zircon. Geochim Cosmochim Acta 64:1905–1923

Hoskin PWO, Schaltegger U (2003) The composition of zircon and igneous and metamorphic petrogenesis. In: Hanchar JM, Hoskin PWO (eds) Zircon, reviews in mineralogy and geochemistry, vol 53. Mineralogical Society of America, Washington, pp 27–62

Howard KA, Wooden JL, Simpson RW, Pease VL (1996) Extension-related plutonism along the Colorado River extensional corridor. Geol Soc Am Abstr Program 28:450

La Tourrette TZ, Burnett DS, Bacon CR (1991) Uranium and minor-element partitioning in Fe–Ti oxides and zircon from partially melted granodiorite, Crater Lake, Oregon. Geochim Cosmochim Acta 55:457–469

Leslie S, Miller J, Miller C, Wooden J, Faulds J (2007) Magmatic construction of the Searchlight magmatic system (Eldorado-Newberry Mountains, Nevada) as revealed through zircon geochemistry and Ti-in-zircon geothermometry. Eos Trans AGU 88:V51C-0707

Luo Y, Ayers JC (2009) Experimental measurements of zircon/melt trace element partition coefficients. Geochim Cosmochim Acta 73:3656–3679

Mahood GA, Hildreth W (1983) Large partition coefficients for trace elements in high-silica rhyolites. Geochim Cosmochim Acta 47:11–30

Marks MAW, Coulson AM, Schilling J, Jacob DE, Schmitt AK, Markl G (2008) The effect of titanite and other HFSE-rich mineral (Ti-bearing andradite, zircon, eudialyte) fractionation on the geochemical evolution of silicate melts. Chem Geol 257:153–172

Mazdab FK, Wooden JL (2006) Trace element analysis of accessory and rock forming minerals by ion microprobe (SHRIMP-RG). Eos Trans AGU 87:V33A-0630

Miller JS, Wooden JL (2004) Residence, resorption and recycling of zircons in Devils Kitchen rhyolite, Coso Volcanic field, California. J Petrol 45:2155–2170

Miller CF, McDowell SM, Mapes RW (2003) Hot and cold granites? Implications of zircon saturation and preservation of inheritance. Geology 31:529–532

Miller JS, Matzel JEP, Miller CF, Burgess SD, Miller RB (2007a) Zircon growth and recycling during the assembly of large, composite arc plutons. J Volcanol Geotherm Res 167:282–299

Miller JS, Matzel J, Wooden JL, Burgess S, Mazdab FK, Mundil R (2007b) Zircon age spectra, zircon crystallization temperature, and the growth of the half dome and cathedral peak granodiorites, Sierra Nevada batholith, California. Geol Soc Am Abstr Program 39:527

Pallister JS, Hoblitt RP, Reyes AG (1992) A basalt trigger for the 1991 eruptions of Pinatubo volcano? Nature 356:426–428

Putnis A, Fernandez-Diaz L, Prieto M (1992) Experimentally produced oscillatory zoning in the (Ba, Sr)SO_4 solid solution. Nature 358:743–745

Reid MR, Vazquez JA (2006) Crystal-scale t-T-X records in zircons from the Youngest Toba Tuff, Sumatra, Indonesia, Eos Trans. AGU 87:V54B-01

Reid MR, Coath CD, Harrison TM, McKeegan KD (1997) Prolonged residence times for the youngest rhyolites associated with Long Valley Caldera: (super 230) Th- (super 238) U ion microprobe dating of young zircons. Earth Planet Sci Lett 150:27–39

Reid MR, Vazquez JA, Simon JI, Schmitt AK (2006) Zircon geothermometry and the Bishop Tuff: Evidence for remobilization of crystal mush or for temperature-independent Ti partitioning? Eos Trans. AGU 87:V51E-1712

Rubatto D, Hermann J (2007) Experimental zircon/melt and zircon/garnet trace element partitioning and implications for the geochronology of crustal rocks. Chem Geol 241:38–61

Schmitt AK, Lindsay JM, de Silva S, Trumbull RB (2003) U-Pb zircon chronostratigraphy of early-Pliocene ignimbrites from La Pacana, North Chile: Implication for the formation of stratified magma chambers. J Volcanol Geotherm Res 120:43–53

Shore M, Fowler AD (1996) Oscillatory zoning in minerals: a common phenomenon. Can Mineral 34:1111–1126

Sparks SRJ, Sigurdsson H, Wilson L (1977) Magma mixing: a mechanism for triggering acid explosive eruptions. Nature 267:315–318

Tomkins HS, Powell R, Ellis DJ (2007) The pressure dependence of the zirconium-in-rutile thermometer. J Metamorph Geol 25:703–713

Vazquez JA, Reid MR (2002) Timescales of magma storage and differentiation of voluminous high-silica rhyolites at Yellowstone caldera, Wyoming. Contrib Mineral Petrol 144:274–285

Vazquez JA, Reid MR, Kyriazis SF (2006) Differentiation and thermal history of the post-collapse magma reservoir at Yellowstone caldera as revealed by combining the temperature-age-compositional history of zircons. Eos Trans AGU, 87:V51E-1713

Vazquez JA, Kyriazis S, Reid MR, Sehler R, Ramos F (2008) Thermochemical evolution of young rhyolites at Yellowstone: evidence for a cooling but periodically replenished postcaldera magma reservoir. J Volcanol Geotherm Res (in press)

Walker BA, Miller CF, Claiborne LL, Wooden JL, George B (2007) Batholith construction: New insights concerning timescales and physical processes from the Spirit Mountain batholith, southern Nevada. J Volcanol Geotherm Res 167:239–262

Wark DA, Miller CF (1993) Accessory mineral behavior during differentiation of a granite suite: monazite, xenotime and zircon in the Sweetwater Wash pluton, southeastern California, USA. Chem Geol 110:49–67

Wark DA, Hildreth W, Spear FS, Cherniak DJ, Watson EB (2007) Pre-eruption recharge of the Bishop magma system. Geology 35:235–238

Watson EB (1980) Some experimentally determined zircon-liquid partition coefficients for the rare-earth elements. Geochim Cosmochim Acta 44:895–897

Watson EB (1996) Dissolution, growth and survival of zircons during crustal fusion: kinetic principles, geological models, and implications for isotopic inheritance. Special Paper. Geol Soc Am 31:43–56

Watson EB, Harrison TM (1983) Zircon saturation revisited: temperature and composition effects in a variety of crustal magma types. Earth Planet Sci Lett 64:295–304

Watson EB, Harrison TM (2005) Zircon thermometer reveals minimum melting conditions on earliest Earth. Science 308:841–844

Watson EB, Wark DA, Thomas JB (2006) Crystallization thermometers for zircon and rutile. Contrib Mineral Petrol 151:413–433

Wiebe RA, Hawkins DP (2004) Multiple replenishments in an evolving silicic magma chamber: the Vinalhaven intrusive complex, Maine, USA. Geochim Cosmochim Acta 68:A672

Wilson CJN, Blake S, Charlier BLA, Sutton AN (2006) The 26.5 Oruanui eruption, Taupo Volcano, New Zealand: development, characteristics and evacuation of a large rhyolite magma body. J Petrol 47:35–69